JOURNAL OF PETROLOGY | VOLUME 39 | NUMBER 3 | PAGES 439–468 | 1998

A Liquid Line of Descent of the Jotunite (Hypersthene Monzodiorite) Suite

JACQUELINE VANDER AUWERA[1]*, JOHN LONGHI[2] AND JEAN-CLAIR DUCHESNE[1]

[1]L.A. GÉOLOGIE, PÉTROLOGIE ET GÉOCHIMIE, UNIVERSITÉ DE LIÈGE, B-4000 LIÈGE, BELGIUM

[2]LAMONT–DOHERTY EARTH OBSERVATORY, PALISADES, NY 10964, USA

RECEIVED JANUARY 10, 1997; REVISED TYPESCRIPT ACCEPTED SEPTEMBER 30, 1997

Proterozoic massif anorthosites are usually associated with variable amounts of a characteristic suite of rocks ranging from a melanocratic facies highly enriched in Fe, Ti and P (FTP rocks) to mafic and granitic rocks (the jotunite–charnockite suite). Here experimental and geochemical data on fine-grained (chilled) samples from several intrusions of the Rogaland Province are used to decipher their petrogenesis. Modeling of these data supports the hypothesis that extensive fractionation of primitive jotunites can produce quartz mangerites with REE concentrations in the range of jotunites, strong depletions in U, Th, Sr and Ti, and smaller to no relative depletions in Hf and Zr. Experimental and petrographic data indicate that the FTP rocks represent accumulations of a dense oxide–apatite–pigeonite assemblage from coexisting multisaturated jotunitic to mangeritic liquids. The Rogaland jotunitic–charnockitic trend corresponds to a multi-stage process of polybaric fractional crystallization and crystal accumulation. The early stage, in which a primitive jotunitic magma fractionates to produce an evolved jotunite, probably took place several kilometers below the intrusion level of dikes, either in mafic chambers similar to that of the Bjerkreim–Sokndal layered intrusion or in masses of crystallizing andesine anorthosite. The later stage of fractionation, which may have involved flow differentiation, took place within the dikes themselves and produced compositions ranging from evolved jotunite to mangerite to quartz mangerite and charnockite.

KEY WORDS: *anorthosite*; *experimental petrology*; *geochemistry*; *monzodiorite*; *Rogaland anorthosite complex*

INTRODUCTION

Proterozoic massif anorthosites are usually associated with variable amounts of a characteristic suite of mafic to granitic rocks. The least evolved rocks of this suite are enriched in mafic minerals (low- and high-Ca pyroxenes, Fe–Ti oxides, apatite), and in some cases very high concentrations of these phases give rise to melanocratic rocks. Various names including ferrodiorite, monzonorite, jotunite, Fe–Ti–P-rich rocks (FTP) and oxide–apatite gabbronorite have been used; however, in this study, we will refer to them by the collective term of jotunite (hypersthene monzodiorite). Evolved rocks of the suite include mangerites (hypersthene monzonite), quartz mangerites and charnockites (hypersthene granite). We will refer to the suite as a whole as the jotunite suite.

The origin of jotunites remains the subject of considerable debate, despite their similar textural and geochemical characteristics from one anorthosite complex to another. Several hypotheses, not mutually exclusive, have been proposed: (1) jotunites are residual liquids after anorthosite crystallization (Ashwal, 1982; Morse, 1982; Wiebe, 1990; Emslie *et al.*, 1994); (2) they are the parental magmas of the andesine anorthosite suite (Duchesne *et al.*, 1974; Duchesne & Demaiffe, 1978; Demaiffe & Hertogen, 1981); (3) they are products of partial melting of the lower crust (Duchesne *et al.*, 1985, 1989; Duchesne, 1990); (4) they are transitional rocks in a comagmatic sequence from anorthosite to mangerite (Wilmart *et al.*, 1989; Owens *et al.*, 1993; Duchesne & Wilmart, 1997); (5) they are derived by fractionation of mafic magmas unrelated to the anorthositic suite (Emslie, 1985); (6) they are immiscible liquids conjugate to

*Corresponding author. Telephone: +32 4 3662253. Fax: +32 4 3662921. e-mail: jvdauwera@ulg.ac.be

mangerites (Philpotts, 1981). In this paper, we present new experimental data on two jotunite samples from the same dike (the Varberg dike) in the Rogaland anorthositic complex as well as new geochemical data (major and trace elements) on fine-grained (chilled) jotunitic rocks from other intrusions in the Rogaland Province. We then use these data as well as published experimental and geochemical data from the literature to: (1) define a liquid line of descent extending from jotunite up to quartz mangerite (or acidic rocks); (2) discuss the possible origins of rocks showing extreme concentrations of FeO, TiO_2 and P_2O_5; and (3) develop models of major and trace element [REE (rare earth elements), Sr, U, Th, Zr, Hf, Ta, Rb, Co, Ni, Cr, Sc] fractionation within the suite.

GEOLOGICAL SETTING AND PETROGRAPHY

The Rogaland intrusive complex of southern Norway (Fig. 1) (Michot, 1960; Michot & Michot, 1969) is one of the group of Proterozoic anorthositic provinces that have been recognized world-wide (Ashwal, 1993). Massif-type anorthosites (Egersund–Ogna; Håland–Helleren; Åna–Sira), leuconoritic bodies (Hidra, Garsaknatt) and a large layered intrusion (Bjerkreim–Sokndal: BKSK) occupy most of the surface exposure. Jotunitic rocks mainly occur in a system of dikes and small intrusions (Duchesne *et al.*, 1985, 1989). There are also several Fe–Ti ore bodies within the complex (Krause & Pedall, 1980; Duchesne, 1998). New U–Pb ages obtained from zircon and baddeleyite (Schärer *et al.*, 1996) suggest that emplacement of this complex occurred within <10 my (between 930 and 920 Ma).

The Rogaland jotunitic suite was first described by Michot (1960) and then extensively studied by Duchesne, Demaiffe and coworkers in several papers reviewed by Duchesne (1990). The characteristics of jotunites will only be briefly summarized here. Jotunites are typically medium grained (from 0·1 mm to a few millimeters in size) and contain plagioclase (usually antiperthitic), some perthitic K-feldspar, poikilitic inverted pigeonite, augite, Fe–Ti oxides, and apatite; these minerals plus meso-perthitic K-feldspar and quartz are characteristic of the evolved facies (Duchesne, 1990). Jotunitic rocks occur mostly as dikes crosscutting massif-type anorthosites but those that have been dated have similar absolute ages in the range of 920–930 Ma (Schärer *et al.*, 1996). Among them, the Tellnes dike in the Åna–Sira massif as well as the Varberg and Lomland dikes in the Egersund–Ogna massif (Fig. 1) have been studied in the most detail (Duchesne *et al.*, 1985; Wilmart *et al.*, 1989). The Tellnes dike, to which we will frequently refer in this study, varies continuously from jotunitic to charnockitic lithologies. It has a well-defined Rb–Sr whole-rock isochron and its compositional variation can be explained by a process of fractional crystallization without progressive contamination (Wilmart *et al.*, 1989). However, whole-rock Rb–Sr isotopic data from other dikes such as Lomland do not fit tightly to isochrons and there is considerable variation in I_{Sr} from dike to dike (0·704–0·710) that does not correlate with other geochemical parameters (Demaiffe *et al.*, 1986; Duchesne *et al.*, 1989), which taken together suggest variable contamination of multiple sources. Jotunites also form small intrusions (e.g. Eia–Rekefjord: Fig. 1) as well as chilled margins to the Hidra and Garsaknatt leuconoritic bodies (Demaiffe & Hertogen, 1981) and, locally, to the Bjerkreim–Sokndal layered intrusion (Duchesne & Hertogen, 1988; Wilson *et al.*, 1996). Experiments on a sample from one of these chilled margins, the Tjörn facies [sample 80123a of Duchesne & Hertogen (1988)], have shown the near-liquidus assemblages to be plagioclase (An_{49}) + olivine (Fo_{64}) at 5 kbar and plagioclase (An_{47}) + low-Ca pyroxene (En_{66}) at 7 kbar (Vander Auwera & Longhi, 1994). The compositions of most of the Rogaland jotunitic suite form coherent trends in variation diagrams (Fig. 2), but the least differentiated compositions (high MgO, low K_2O) are chilled margin samples and form a group distinct from the rest of the dike system. In the following, we will refer to the distinctive group of chilled margin samples as primitive jotunites and to the least differentiated samples of the dike trend as evolved jotunites. In this latter group, most samples are chilled margins to the dikes (75202F, 8926, 89115, 7355).

In this study, we took special care to select samples from different occurrences which probably represent liquid compositions [very fine-grained texture (<250 μm), non-porphyritic facies, elongated apatite and oxide grains randomly dispersed in the other minerals, etc.] and their exact locations are given in Table 1. Three of these samples (80123a, 91141 and 7234: Table 1) from the chilled margin of BKSK and Hidra are primitive jotunites. The remainder of the samples are from the dikes and have compositions ranging from evolved jotunite to quartz mangerite. Although the Varberg dike (Fig. 1) displays the typical mineralogy of jotunites (see above), it contains a chilled margin (Table 1: sample 75202F), which has been observed at several places along its contact, as well as a locally developed, Fe–Ti–P-rich melanocratic facies (sample 75372: TiO_2 6·23%; FeO_t 27·43%; P_2O_5 4·20%) in the interior, where mafic minerals (inverted pigeonite, augite, ilmenite, magnetite, apatite) make up ~75% of the rock, and plagioclase and perthitic K-feldspar make up the remaining 25%. Mineral phases from samples taken along strike of the dike have been analyzed with the electron microprobe to test for geographical variations in mineral compositions.

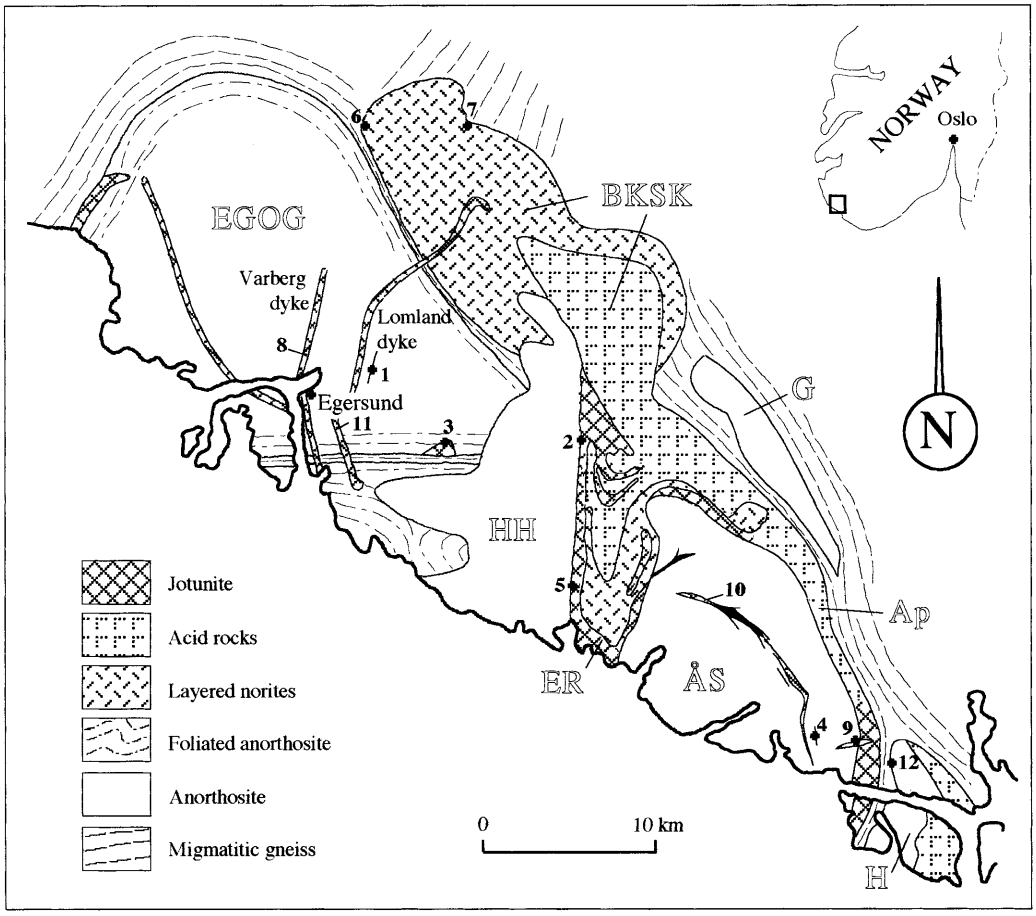

Fig. 1. Schematic geological map of the Rogaland anorthositic complex [after Michot & Michot (1969) and Bolle (1996)]. EGOG, Egersund–Ogna; HH, Håland–Helleren; ÅS, Åna–Sira; H, Hidra; G, Garsaknatt; ER, Eia–Rekefjord; BKSK, Bjerkreim–Sokndal, Ap, Apophysis. Numbers refer to samples described in Table 1.

SAMPLE PREPARATION, EXPERIMENTAL AND ANALYTICAL METHODS

Experiments were carried out on two powdered rocks of the Varberg dike at Lamont–Doherty either in a standard 1/2 inch piston cylinder apparatus or in a Deltech vertical quenching furnace, following the methods described by Fram & Longhi (1992) and Vander Auwera & Longhi (1994). One sample was from the chill margin (sample 75202F; VB); the other was from the melanocratic facies (sample 75372; MEL). High-pressure experiments were run in graphite capsules at 5 kbar (runs VB-1 to VB-5, VB-13 and VB-14 on sample VB, and runs MEL-1 to MEL-3 on sample MEL), the likely pressure of emplacement of the Rogaland intrusive complex (Jansen *et al.*, 1985; Vander Auwera & Longhi, 1994). Dry run conditions are consistent with the relatively low $f(H_2O)$ that is a general feature of massif anorthosites and related rocks (see, e.g. Morse, 1982). However, the graphite capsules imposed a relatively low oxygen fugacity in these experiments, probably between FMQ (fayalite–magnetite–quartz) – 2 and FMQ – 4 (Vander Auwera & Longhi, 1994), which inhibits magnetite stability. To aproximate the $f(O_2)$ of the jotunites and to determine the effects of magnetite, which is a late-stage mineral in the primitive jotunites, on the liquid line of descent, we also performed a few 1 atm melting experiments in a controlled CO–CO_2 atmosphere. These were carried out at two different $f(O_2)$ values: NNO (nickel–nickel oxide; runs VB-16 and VB-17) and FMQ (run VB-6); $f(O_2)$ was measured with a Ca-doped ZrO_2 electrolyte cell. Good agreement was found between $f(O_2)$ determined directly and $f(O_2)$ calculated by applying the Andersen & Lindsley (1988) model to the compositions of coexisting ilmenite and spinel produced in the experiments. To minimize

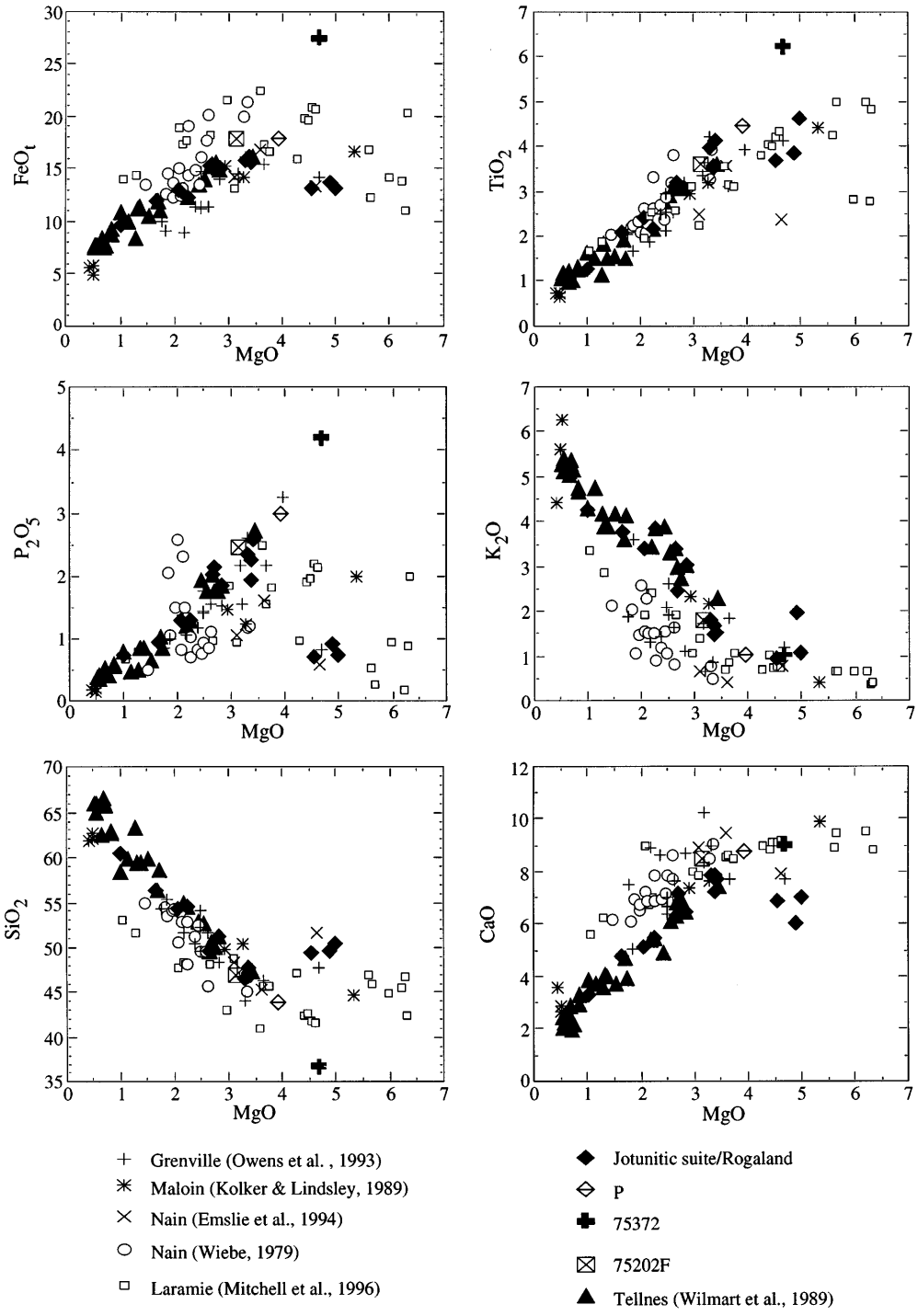

Fig. 2. Major element variation diagrams of the jotunitic suite. Data from fine-grained samples (chills), from the Tellnes dike (Wilmart, 1988; Wilmart *et al.*, 1989) and from other localities [Grenville Province, Quebec: Owens *et al.* (1993); Laramie: Kolker & Lindsley (1989); Mitchell *et al.* (1996); Nain: Wiebe (1979); Emslie *et al.* (1994)] are shown for comparison. P corresponds to the average of four samples from the Puntervoll facies (FTP rocks) of the Lomland dike (Duchesne *et al.*, 1985).

Table 1: Sample description, location and facies of jotunites

Sample	UTM grid: zone 32 VLK	Intrusion
89115/ch (1)*	305–859	Kjervall dike crosscutting the Egersund–Ogna anorthosite
78211/ch (2)	407–825	Eiavatn dike crosscutting the Eia–Rekefjord intrusion
8925, 8926/ch (3)	315–812	dike on top of the Koldal small intrusion: 8925 is from the central part of the dike, and 8926 from the contact
8951/ch (4)	534–615	satellite to the Tellnes dike crosscutting the Åna–Sira anorthosite
7355/ch (5)	399–727	Eia–Rekefjord intrusion
91141/ch (6), 80123a/ch (7)†	273–992; 354–983	fine-grained margin of the Bjerkreim–Sokndal intrusion
75182, 7519, 75202F/ch, 75202G, 75204, 75206, 75372, 78201, 7912(8)	249–883; 249–875; 244–825; 244–825; 244–825; 244–825; 244–838; 251–797; 243–841	Varberg dike crosscutting the Egersund–Ogna anorthosite
7838/ch, 8034/ch (9)	550–624; 554–627	Fidsel dike crosscutting the Apophysis
T2/ch,T221/ch,T82/ch, 7832, 7828, 7252 (10)‡	514–657; 455–701; 517–653; 523–627; 472–698; 477–697	Tellnes dike crosscutting the Åna–Sira anorthosite
66175, 7536, 7533, 7534 (11)	263–803; 267–815; 275–827; 273–829	Puntervold facies (melanorites) of the Lomland dike
7234/ch (12)§	589–602	fine-grained margin of the Hidra leuconoritic body

*Numbers in parentheses correspond to the localities shown in Fig. 1; /ch indicates that the sample corresponds to a chill. †Duchesne & Hertogen (1988). ‡Wilmart (1988). §Duchesne *et al.* (1974).

iron loss in highly crystalline runs, powdered samples were pressed into disks of 6 mm diameter (bonded with polyvinyl alcohol) and loosely wrapped in Pt wire of 0·254 mm diameter. Run conditions and phase assemblages are given in Table 2.

Analytical method

After each experiment, the charges were mounted in epoxy, polished and analyzed at Lamont–Doherty under the Camebax/Micro electron microprobe equipped with a wavelength dispersive system. Accelerating voltage was set at 15 kV and all elements were measured for 20 s at a beam current of 25 nA, except in the case of feldspars, phosphates, and glasses, where Na and K were measured first for 30 s at 5 nA. Rims of minerals were analyzed with a point beam and glasses with a defocused beam of 5 μm to minimize alkali loss. X-ray intensities were reduced using the Cameca PAP correction program. A combination of mineral and glass standards were used for glass analyses whereas only mineral standards were used for plagioclase, oxides, pyroxenes, and olivines. Major element compositions of the experimental phases are reported in Table 3. Rims and cores of feldspars and pyroxenes occurring in the different facies of the Varberg dike have been analyzed with the Cameca SX50 of the CAMST ('Centre d'Analyse par Microsonde pour les Sciences de la Terre', Louvain-La-Neuve, Belgium; J. Wautier analyst). Standards included natural minerals and synthetic compounds. Accelerating voltage was set at 15 kV and beam current was 20 nA with 10 s counting times. X-ray intensities were reduced using the Cameca PAP correction program. Results are given in Table 4.

Mass balance between the bulk composition of the starting material and the compositions of all phases present in each run has been calculated using a least-squares multiple regression to determine phase proportions and to test if Fe and Na loss occurred in the 1 atm experiments. Results are given in Table 2. Na loss ranges from 4% up to 14% whereas Fe displays a small gain in VB-16 (6%) and a significant one in VB-17 (25%). The latter experiment did not equilibrate pervasively, as the temperature was near the solidus and the charge melted only locally. In run VB-14, the orthopyroxene (opx) coefficient had a negative sign. The opx coefficient

Table 2: Experimental conditions and products

Experiment	T (°C)	P	t (h)	$f(O_2)$	Products
VB-1	1150	5 kbar	25		gl
VB-2	1120	5 kbar	26		gl_{94} pl_6
VB-3	1100	5 kbar	36		gl_{96} pl_4
VB-4	1080	5 kbar	47		gl_{82} pl_{17} $ol_{0.2}$ $il_{0.7}$ $ap_{0.1}$
VB-14	1078	5 kbar	66		gl_{61} pl_{30} pig_6 il_3 $ap_{0.01}$ opx $_0$
VB-13	1074	5 kbar	114		gl pl ol il ap pig
VB-5	1060	5 kbar	71		gl pl pig aug il ksp qtz
VB-6	1050	1 bar	125	FMQ	gl_{50} pl_{30} ol_7 il_3 $uvsp_6$ phosph
VB-16	1065	1 bar	46	NNO	gl_{47} pl_{28} pig_4 aug_4 $uvsp_{13}$ $phosp_4$
VB-17	1060	1 bar	89	NNO	gl_{30} pl_{33} pig_4 aug_9 $uvsp_{19}$ $phosp_5$
MEL-1	1130	5 kbar	23		gl
MEL-2	1110	5 kbar	18		gl_{99} il_1
MEL-3	1090	5 kbar	25		gl_{90} il_4 ol_4 ap_2

The numbers following the phase abbreviations are the weight proportions of the relevant phases present in the experiments, calculated using a weighted least-squares minimization.

was then changed to zero and its components were included in the other phases. This results in an increased proportion of the remaining phases.

The fine-grained samples of jotunites were analyzed for major elements and some trace elements by X-ray fluorescence on a CGR Lambda 2020 Spectrometer at the University of Liège (analyst G. Bologne) (Bologne & Duchesne, 1991). The other trace elements were analyzed either on a VG elemental PQ2 Plus inductively coupled plasma-mass spectrometer at the University of Liège (Vander Auwera *et al.*, 1998) or by neutron activation at the Pierre Süe Laboratory (CEA, Saclay, France; analyst J. L. Joron). Major and trace element data are presented in Table 5.

EXPERIMENTAL AND ANALYTICAL RESULTS

Mineral compositions

The compositions of plagioclase and pyroxenes from the Varberg dike (Fig. 3) have a limited range and are similar to those observed in jotunites from the Tellnes dike (Wilmart, 1988). In the chill margin plagioclase is not significantly zoned, with cores of An_{33} and mantles with an average of An_{34}. Augite, whether as lamellae or primary crystals, has an intermediate *mg*-number (0·49). The low-Ca pyroxene (lpyx) is orthopyroxene ($Wo_{1\cdot2}Ens_{35}$) inverted from pigeonite (Fig. 3, Table 4). In the sample of the melanocratic facies (MEL), the pyroxenes are similar to those elsewhere in the dike, but alkali feldspar is present ($An_{0\cdot6}Or_{89}$) together with plagioclase ($An_{32}Ab_{66}Or_2$). There seems to be a correlation between plagioclase composition and bulk composition, as plagioclase displaying the lowest anorthite content (An_{30} in sample 75206; Table 4) is associated with the bulk composition showing the lowest MgO (2·79%) and highest SiO_2 (49·29%) content observed in the samples from the Varberg dike (Table 5; analysis of sample 75204 is given instead of that of sample 75206). This observation is supported by petrographic data from the Tellnes dike, in which there is a systematic change in the feldspar composition associated with bulk composition: jotunites are characterized by antiperthitic plagioclase and lesser K-feldspar (microperthite), mangerites contain more K-feldspar and mesoperthite-rimmed plagioclase, whereas quartz mangerites display mesoperthite (Wilmart *et al.*, 1989).

Experimental results

At 5 kbar and 1120°C plagioclase (An_{49}) is the sole liquidus phase of VB, the chill margin sample. Olivine (Fo_{50}), ilmenite, and apatite appear approximately together at 1080°C in run VB-4. The SiO_2 and P_2O_5 concentrations in the 1080°C liquid are 46·0% and 2·74%, respectively (Table 3); these values are consistent with the apatite-saturation model of Harrison & Watson (1984). In run VB-14 at 1078°C there is a drastic increase in crystallinity and olivine is replaced by pigeonite and orthopyroxene. At a slightly lower temperature (1074°C, VB-13) olivine reappears as a stable phase. Only the top half of the VB-13 charge shows signs of glass and textural equilibration. Thus the solidus probably lies within the

Table 3: Composition of experimental products

Exp.	No.	Ph	SiO_2	TiO_2	Al_2O_3	Cr_2O_3	Fe_2O_3	FeO	MgO	MnO	CaO	K_2O	Na_2O	P_2O_5	F	Total	'An, Fo, En'
VB-1	4	gl	47·26(34)	3·82(9)	13·97(9)			15·56(19)	3·06(8)	0·25(3)	7·70(3)	1·77(3)	3·28(6)	2·4(4)		99·07	
VB-2	4	gl	47·62(31)	3·85(10)	13·30(14)			16·34(22)	3·16(3)	0·23(2)	7·47(11)	1·92(3)	2·95(11)	2·43(2)		99·27	
	5	pl	57·29(60)	0·15(2)	27·52(47)			0·57(7)	0·06(1)	0·00	9·56(34)	0·78(5)	5·61(32)	0·00		101·55	46
VB-3	4	gl	47·51(26)	3·9(2)	13·47(11)			15·74(14)	3·16(3)	0·23(1)	7·57(5)	1·89(3)	3·17(9)	2·53(5)		99·17	
	3	pl	56·30(28)	0·14(5)	27·89(47)			0·57(7)	0·07(2)	0·00	9·99(79)	0·62(8)	5·44(18)	0·00		101·01	49
VB-4	4	gl	46·00(52)	4·24(12)	11·57(21)			18·26(46)	3·66(7)	0·27(2)	7·80(11)	1·82(8)	2·80(1)	2·74(8)		99·16	
	4	pl	58·5(1·4)	0·05(6)	26·80(99)			0·52(9)	0·03(2)	0·00	8·8(1·2)	0·82(21)	5·88(55)	0·00		101·36	43
	5	ol	34·18(19)	0·22(3)	0·05(1)	0·01(1)		41·44(27)	23·38(21)	0·51(2)	0·40(3)	0·00	0·02(1)	0·00		100·21	50
	4	il	0·05(2)	55·93(4)	0·33(3)	0·00	0·00	40·42(9)	4·20(6)	0·41(2)	0·19(5)	0·00	0·02(1)	0·00		101·55	
	3	ap	0·00	0·00	0·02(3)			0·97(23)	0·18(13)	0·06(0)	53·52(73)	0·08(6)	0·06(1)	41·14(19)	1·85(51)	97·88	
VB-14	7	gl	45·80(36)	4·16(8)	10·87(8)			20·17(22)	3·25(7)	0·32(3)	7·49(7)	2·04(9)	2·69(8)	2·84(7)		99·63	
	7	pl	59·60(72)	0·02(3)	25·81(33)			0·39(11)	0·02(1)	0·00	7·24(31)	1·46(51)	5·65(31)	0·00		100·19	38
	8	pig	50·93(55)	0·83(14)	1·1525)	0·01(1)		26·25(77)	16·41(44)	0·51(4)	4·19(56)		0·08(1)			100·36	48
	5	il	0·05(2)	54·35(27)	0·32(2)	0·01(1)	0·00	41·76(17)	3·39(8)	0·42(4)	0·11(5)		0·01(1)			100·42	
	1	opx	50·50	0·31	0·80			29·46	15·68	0·67	1·85		0·06			99·33	47
	4	ap	0·00	0·00	0·00			0·94(48)	0·20(21)	0·08(2)	54·27(51)	0·03(1)	0·07(2)	40·92(28)	1·93(55)	98·44	
VB-13	2	gl1	50·24(1·1)	2·92(8)	10·48(3)			19·58(48)	1·85(4)	0·33(6)	6·52(5)	2·72(4)	2·84(32)	2·47(3)		99·95	
	1	gl2	51·01	2·61	10·92			17·15	1·59	0·32	7·32	3·20	3·07	3·28		100·47	
	1	gl3	55·18	2·33	11·79			15·58	1·39	0·22	5·12	4·04	4·68	1·73		102·06	
	3	gl4	50·50(87)	2·82(19)	10·63(25)			18·77(1·4)	1·76(15)	0·33(4)	6·79(46)	2·88(28)	2·91(26)	2·74(47)		100·13	
	9	pl	59·80(57)	0·06(7)	25·59(33)			0·41(14)	0·02(2)	0·00	7·14(40)	1·52(46)	5·70(24)	0·00		100·24	37
	7	pig	49·84(69)	0·79(7)	0·95(19)	0·01(1)		30·89(91)	12·70(60)	0·59(4)	4·42(62)		0·08(2)			100·27	38
	1	ol	31·96	0·46	0·04	0·06		54·39	12·07	0·75	0·61		0·02			100·36	28
	5	il	0·08(2)	53·17(38)	0·21(1)	0·02(2)	0·00	43·63(27)	1·98(3)	0·43(5)	0·17(9)		0·02			99·71	
	5	ap	0·00	0·00	0·05(3)			1·24(12)	0·23(1)	0·08(4)	52·64(38)	0·06(1)	0·07(2)	40·84(48)	2·15(20)	97·36	
VB-5	3	gl	67·64(1·4)	0·77(11)	14·85(2·0)	0·01(1)		4·49(1·3)	0·32(9)	0·04(2)	1·47(17)	6·17(77)	3·70(42)	0·31(5)		99·77	

Table 3: continued

Exp.	No.	Ph	SiO_2	TiO_2	Al_2O_3	Cr_2O_3	Fe_2O_3	FeO	MgO	MnO	CaO	K_2O	Na_2O	P_2O_5	F	Total	'An, Fo, En'
VB-6	6	gl	54·41(64)	2·54(6)	12·18(11)	0·00		14·16(31)	2·22(4)	0·25(3)	6·11(11)	2·92(15)	3·00(24)	1·86(6)		99·65	
	11	pl	59·04(1·3)	0·07(5)	26·22(77)	0·00		0·65(20)	0·04(3)	0·00	8·27(92)	1·05(19)	5·46(55)	0·00		100·80	43
	5	ol	34·49(51)	0·19(4)	0·13(10)	0·00		42·81(26)	21·64(32)	0·67(4)	0·52(10)		0·03(1)			100·48	47
	4	il	0·03(1)	46·9(3·7)	0·45(21)	0·02(2)	12·65	35·92(2·3)	3·26(10)	0·44(1)	0·14(6)					99·81	
	6	uvsp	0·13(1)	23·88(25)	2·23(3)	0·03(2)	21·05	48·81(61)	2·64(7)	0·47(4)	0·22(6)					99·46	
VB-16	7	gl	56·69(2·0)	2·18(21)	12·53(40)	0·03(2)		11·02(1·2)	2·34(34)	0·22(4)	5·59(66)	2·83(30)	3·06(8)	1·65(32)		98·14	
	12	pl	57·12(1·7)	0·07(5)	26·51(1·1)	0·00		0·56(22)	0·03(3)	0·00	8·9(1·2)	0·80(17)	5·00(58)	0·00		98·97	47
	8	pig	50·76(43)	0·77(8)	1·25(22)	0·02(1)		19·9(1·3)	17·9(1·1)	0·58(3)	7·5(2·1)		0·11(4)			98·85	52
	1	aug	49·57	0·96	1·70	0·05		17·45	15·50	0·48	11·98		0·17			97·86	46
	5	uvsp	0·16(3)	19·76(54)	2·46(6)	0·02(1)	28·10	44·08(53)	2·99(7)	0·50(2)	0·12(7)		0·01(1)			98·20	
	6	phosp	0·00	0·00	0·11(9)			3·45(11)	3·75(4)	0·18(2)	44·90(25)	0·23(23)	0·49(17)	43·87(22)	0·00	96·98	
VB-17	5	gl	66·94(73)	1·24(12)	13·97(7)			5·71(21)	1·03(7)	0·10(2)	2·65(8)	4·13(20)	3·48(15)	0·57(4)		99·82	
	9	pl	58·3(1·5)	0·11(6)	26·52(97)			0·67(27)	0·04(4)	0·00	8·62(91)	0·92(22)	5·00(62)	0·00		100·15	44
	3	pig	51·06(94)	0·61(21)	0·97(40)	0·02(2)		22·6(1·5)	17·3(1·6)	0·73(5)	6·2(2·5)		0·09(4)			99·59	50
	9	aug	50·19(43)	0·88(15)	1·43(20)	0·02(1)		17·8(1·3)	14·1(1·0)	0·58(12)	14·1(2·1)		0·20(3)			99·32	41
	5	uvsp	0·37(25)	16·41(31)	2·32(8)	0·02(1)	35·07	41·73(40)	2·57(12)	0·61(4)	0·29(11)		0·02(1)			99·41	
	4	phosp	0·00	0·00	0·34(16)			3·59(10)	3·72(4)	0·22(2)	45·49(30)	0·24(19)	0·46(13)	43·56(61)	0·00	97·62	
MEL-1	4	gl	36·59(16)	7·08(2)	7·34(4)			27·05(8)	4·51(4)	0·34(3)	9·13(8)	0·62(6)	1·87(8)	4·40(7)		98·93	
MEL-2	5	gl	36·95(37)	6·56(18)	7·13(15)			27·19(39)	4·61(2)	0·37(2)	9·29(7)	0·57(4)	1·66(5)	4·51(8)		98·85	
	4	il	0·04(1)	54·53(25)	0·31(2)	0·01(1)	0·00	41·35(31)	3·66(5)	0·36(1)	0·20(6)	0·00	0·01(1)	0·00		100·47	
MEL-3	6	gl	39·56(21)	5·78(5)	8·14(8)			25·66(28)	3·99(7)	0·35(2)	9·01(7)	0·61(7)	1·98(11)	3·91(8)		98·98	
	5	ol	33·19(16)	0·24(3)	0·03(1)	0·05(1)		46·13(23)	19·36(8)	0·53(3)	0·42(2)	0·00	0·02	0·00		99·98	43
	4	il	0·03(1)	55·38(37)	0·29(2)	0·01(1)	0·00	41·68(26)	3·34(4)	0·43(3)	0·15(2)	0·00	0·00	0·00		101·31	
	3	ap	0·00	0·00	0·01(1)			1·46(40)	0·24(19)	0·05(2)	53·78(41)	0·04(2)	0·04(1)	41·21(51)	1·69(39)	98·52	

gl, glass; ol, olivine; pig, pigeonite; opx, orthopyroxene; pl, plagioclase; il, ilmenite; uvsp, ulvöspinel; aug, augite; ap, apatite; phosp, whitlockite. For each phase, the average of several analyses (No. is the number of analyses) is given and the standard deviation is in parentheses. Fo [Mg × 100/(Mg + Fe)], En [Mg × 100/(Mg + Fe + Ca)], An [Ca × 100/(Ca + Na + K)] are given in atomic units.

Table 4: Microprobe analyses of the Varberg dike feldspars and pyroxenes

Sample:	75202F	7912	7912	75202G	75182	75182	75372	75372	75206	78201
Phase:	Plag	Plag	FK	Plag	Plag	FK	plag	FK	Plag	Plag
No.:*	6	6	2	4	8	2	8	4	7	8
Feldspars										
SiO_2	61·06	60·89	64·88	61·38	61·34	64·33	61·16	64·90	61·81	60·90
Al_2O_3	24·62	24·78	18·29	24·48	24·43	18·40	24·63	18·43	24·16	24·66
FeO	0·21	0·18	0·06	0·15	0·11	0·08	0·12	0·05	0·22	0·10
CaO	6·96	7·15	0·04	6·65	6·65	0·06	6·67	0·11	6·15	7·01
K_2O	0·35	0·36	16·06	0·35	0·36	15·22	0·40	14·77	0·32	0·37
Na_2O	7·38	7·28	0·82	7·43	7·47	0·93	7·49	1·14	7·79	7·30
Total	100·58	100·64	100·15	100·45	100·36	99·01	100·48	99·39	100·45	100·34
Si	2·7032	2·6950	2·9957	2·7160	2·7165	2·9915	2·7075	2·9983	2·7321	2·7008
Al	1·2842	1·2923	0·9952	1·2763	1·2751	1·0082	1·2851	1·0031	1·2586	1·2890
Fe	0·0076	0·0065	0·0025	0·0056	0·0039	0·0030	0·0045	0·0021	0·0080	0·0038
Ca	0·3300	0·3393	0·0019	0·3153	0·3153	0·0030	0·3166	0·0056	0·2914	0·3329
Na	0·6333	0·6246	0·0738	0·6372	0·6416	0·0836	0·6431	0·1023	0·6673	0·6273
K	0·0201	0·0204	0·9457	0·0200	0·0205	0·9027	0·0224	0·8701	0·0181	0·0211
Catsum	4·9783	4·9781	5·0146	4·9704	4·9730	4·9919	4·9791	4·9813	4·9755	4·9748
% An	33·56	34·46	0·19	32·42	32·27	0·30	32·23	0·57	29·83	33·93
% Ab	64·40	63·46	7·22	65·53	65·64	8·45	65·49	10·46	68·32	63·93
% Or	2·04	2·08	92·60	2·06	2·10	91·25	2·28	88·97	1·85	2·15

Table 4: continued

Sample:	75202F	75202F	7912	7912	75202G	75202G	75202G	75182	75182	75372	75372	75206	75206	78201	78201	78201
Phase:	opx	cpx	opx	cpx	opx	cpx	cpx exs.†	opx	cpx	opx	cpx	opx	cpx	opx	cpx	cpx exs.†
No.:*	4	4	4	3	7	3	1	4	3	6	4	4	4	4	2	2
Pyroxenes																
SiO_2	49·84	51·25	49·69	51·45	49·61	51·23	50·98	49·73	51·34	49·74	51·13	50·39	51·92	50·02	51·14	51·50
TiO_2	0·10	0·14	0·06	0·16	0·10	0·21	0·24	0·10	0·17	0·12	0·24	0·07	0·17	0·11	0·25	0·23
Al_2O_3	0·59	1·24	0·58	1·29	0·71	1·26	1·33	0·60	1·16	0·67	1·31	0·61	1·19	0·65	1·33	1·34
Cr_2O_3	0·04	0·02	0·05	0·05	0·03	0·03	0·00	0·03	0·01	0·04	0·06	0·00	0·01	0·04	0·00	0·01
FeO	37·93	17·52	37·74	17·61	37·14	16·65	16·75	39·11	18·28	37·79	17·92	35·06	15·36	37·36	18·97	16·61
MgO	11·69	9·35	11·30	9·02	11·98	9·46	9·35	10·28	8·20	11·03	8·79	13·14	9·96	11·65	9·17	9·59
MnO	0·81	0·39	0·95	0·40	0·76	0·41	0·31	0·84	0·36	0·82	0·37	0·92	0·44	0·82	0·46	0·34
CaO	0·56	20·63	0·77	21·24	0·80	21·34	21·78	0·87	21·27	0·83	19·81	0·64	20·71	0·79	18·84	21·38
K_2O	0·03	0·01	0·00	0·01	0·01	0·01	0·00	0·02	0·01	0·01	0·01	0·00	0·01	0·00	0·00	0·01
Na_2O	0·01	0·33	0·00	0·34	0·00	0·34	0·34	0·00	0·33	0·00	0·34	0·00	0·37	0·00	0·37	0·31
Total	101·61	100·90	101·14	101·58	101·14	100·93	101·07	101·57	101·13	101·05	100·22	100·83	100·25	101·44	100·54	101·32
Si	1·9754	1·9676	1·9800	1·9653	1·9702	1·9627	1·9540	1·9840	1·9756	1·9826	1·9798	1·9849	1·9863	1·9805	1·9735	1·9631
Ti	0·0030	0·0040	0·0019	0·0046	0·0029	0·0062	0·0069	0·0031	0·0048	0·0037	0·0070	0·0020	0·0049	0·0031	0·0074	0·0067
Al	0·0275	0·0561	0·0270	0·0581	0·0334	0·0568	0·0602	0·0283	0·0526	0·0316	0·0597	0·0283	0·0536	0·0302	0·0607	0·0600
Cr	0·0012	0·0007	0·0016	0·0016	0·0010	0·0008	0·0000	0·0009	0·0004	0·0013	0·0018	0·0001	0·0006	0·0012	0·0001	0·0004
Fe	1·2571	0·5625	1·2575	0·5626	1·2334	0·5335	0·5368	1·3047	0·5882	1·2598	0·5803	1·1547	0·4914	1·2369	0·6126	0·5293
Mg	0·6908	0·5352	0·6712	0·5133	0·7091	0·5404	0·5341	0·6114	0·4703	0·6553	0·5072	0·7714	0·5679	0·6877	0·5275	0·5450
Mn	0·0272	0·0126	0·0321	0·0129	0·0256	0·0133	0·0100	0·0282	0·0118	0·0276	0·0120	0·0306	0·0144	0·0276	0·0150	0·0110
Ca	0·0237	0·8486	0·0327	0·8692	0·0341	0·8759	0·8943	0·0372	0·8770	0·0353	0·8220	0·0269	0·8489	0·0333	0·7785	0·8731
K	0·0015	0·0006	0·0001	0·0003	0·0006	0·0004	0·0000	0·0012	0·0005	0·0004	0·0004	0·0000	0·0005	0·0002	0·0000	0·0004
Na	0·0005	0·0248	0·0000	0·0255	0·0000	0·0249	0·0253	0·0000	0·0244	0·0002	0·0254	0·0004	0·0274	0·0002	0·0275	0·0230
Catsum	4·0081	4·0127	4·0040	4·0132	4·0101	4·0150	4·0216	3·9989	4·0055	3·9977	3·9954	3·9991	3·9957	4·0009	4·0027	4·0118
% En	35·03	27·50	34·22	26·39	35·87	27·71	27·18	31·30	24·30	33·60	26·56	39·50	29·76	35·12	27·49	27·99
% Fs	63·76	28·89	64·12	28·93	62·40	27·36	27·32	66·80	30·39	64·59	30·39	59·13	25·75	63·18	31·91	27·18
% Wo	1·20	43·61	1·67	44·69	1·73	44·93	45·51	1·90	45·31	1·81	43·05	1·37	44·49	1·70	40·60	44·84
mg-no.	0·36	0·49	0·35	0·48	0·37	0·50	0·50	0·32	0·44	0·34	0·47	0·40	0·54	0·36	0·47	0·51

*No., number of analyses per sample.
†exs., cpx exsolution in opx.

Table 5: Major and trace analyses of whole rocks

Sample:	75372	66175	7536	P	75202G	7534	7533	7519	78201	7912	89115	8925	75202F	8926	75182	7252†	7355	75204	80123‡	T2†	7234§	78211	91141	T221†	8951	T82†	7828†	8034	7838†	7832
Location in Fig. 1:	8	11	11	11	8	11	11	8	8	8	1	3	8	3	8	10	5	8	7	10	12	2	6	10	4	10	10	9	9	10
Major elements as wt % oxide																														
SiO_2	36·79	42·75	43·50	43·88	44·61	44·62	44·66	45·06	45·40	45·63	46·45	46·90	46·93	47·17	47·31	47·32	47·85	49·29	49·39	49·52	49·53	49·82	50·38	51·16	54·33	54·51	56·38	56·40	60·41	65·7
TiO_2	6·23	4·36	4·80	4·45	4·10	4·20	4·42	4·22	3·70	3·57	3·98	4·14	3·59	3·56	3·59	3·60	3·50	3·43	3·67	3·11	3·82	3·18	4·62	3·08	2·41	2·18	1·90	2·09	1·27	0·99
Al_2O_3	7·16	12·18	13·31	12·89	11·80	12·95	13·13	11·79	12·92	12·75	13·22	13·16	13·45	13·76	12·92	12·80	13·40	13·51	15·81	13·54	14·50	13·13	14·65	13·25	13·66	13·23	14·00	13·87	13·76	13·3
FeO_t	27·43	18·58	17·73	17·81	18·21	17·40	17·52	19·38	17·74	17·24	15·72	15·55	15·35	15·68	17·55	16·04	16·03	15·01	13·11	15·25	13·68	14·98	13·20	14·82	12·96	12·30	11·85	11·87	9·65	7·54
MnO	0·41	0·26	0·27	0·26	0·18	0·24	0·27	0·27	0·25	0·20	0·24	0·22	0·19	0·21	0·27	0·21	0·27	0·22	0·13	0·27	0·17	0·21	0·17	0·22	0·19	0·21	0·16	0·15	0·16	0·11
MgO	4·68	4·26	3·93	3·94	3·62	3·85	3·73	3·70	3·67	3·89	3·30	3·42	3·15	3·38	3·26	3·44	3·38	2·79	4·54	2·66	4·90	2·70	4·98	2·84	2·06	2·26	1·69	1·65	1·01	0·65
CaO	9·02	9·13	8·82	8·76	8·69	8·57	8·50	7·20	7·92	8·68	7·81	7·69	8·44	7·23	7·45	7·43	7·83	7·13	6·87	6·33	6·00	7·17	7·01	6·45	5·09	5·43	4·66	4·74	3·31	2·56
Na_2O	1·67	3·01	3·10	3·26	2·99	3·46	3·47	3·11	3·48	3·62	3·54	3·32	3·44	3·63	3·64	3·53	3·72	3·41	3·50	3·14	3·50	3·02	3·53	3·09	2·80	3·58	3·31	3·78	3·41	3·07
K_2O	1·02	0·90	0·90	1·02	1·72	1·21	1·05	1·80	1·37	1·72	1·79	1·52	1·80	1·70	1·81	2·28	1·49	2·20	0·96	3·41	1·95	2·46	1·07	3·03	3·38	3·85	3·60	3·77	4·24	5·04
P_2O_5	4·20	3·40	2·98	2·99	3·10	2·89	2·70	2·40	2·42	2·98	2·35	2·59	2·50	2·26	2·47	2·74	1·95	2·06	0·71	2·03	0·91	2·15	0·73	1·84	1·31	1·29	1·04	0·95	0·75	0·51
Total	98·61	98·83	99·34	99·25	99·02	99·39	99·45	98·93	98·87	100·28	98·40	98·51	98·84	98·58	100·27	99·39	99·42	99·05	98·69	99·26	98·96	98·82	100·34	99·78	98·19	98·84	98·59	99·27	97·97	99·5
Trace elements as ppm																														
Ni	<10	<10	<10	—	40·7	<10	21	—	—	17	—	—	16	—	—	6·60	—	25	60	23	55	—	—	3	—	11	1·4	—	—	—
Cr	3·15	2·71	—	—	76·2	1·88	—	—	—	—	—	—	66·0	—	—	22·0	—	65·7	28·0	48·8	31·8	—	—	—	—	60	34	4	1	21
V	219	171	152	160	176	151	164	—	—	178	109	187	159	164	—	128	231	116	216	87	300	142	284	66	78	60	35	—	—	72
Co	56·0	51·0	45·0	45·8	41·1	40·0	47·0	—	—	24·0	48·9	56·9	34·7	51·1	—	36·0	49·6	30·9	49·0	27·1	46·5	47·1	72·9	30·8	35·1	23	17	20·2	11·5	7·2
Zn	306	200	213	202	234	176	218	—	—	216	214	226	190	233	—	197	—	212	144	258	—	—	133	223	204	243	186	—	—	151
Ga	—	—	—	—	—	—	—	—	—	—	31·6	30·7	—	36·1	—	—	30·4	—	—	—	—	32·1	21·7	—	33·9	—	—	—	—	—
Rb	6·4	5·1	3·7	5·3	8·5	6·9	5·6	10·6	7·0	9·0	10·6	12·7	10·6	12·6	13·0	17·0	16·6	20·4	18·0	25·4	43·0	28·5	5·8	19·2	37·0	39	34	34·0	48·0	71·0
Sr	268	438	485	458	380	473	436	399	431	438	465	463	415	465	375	354	412	375	530	342	382	341	461	349	311	316	272	310	211	128
Y	110	53	52	51	98	45	52	75	63	70	64	69	72	57	69	79·0	107	87	22	95	—	70	33	78	65	95	78	66	68	52
Zr	402	56	21	55	205	85	56	663	221	148	253	203	191	402	598	442	509	250	262	687	300	473	241	598	620	626	717	952	1251	1387
Nb	—	—	—	—	—	—	—	—	—	—	39·9	43·6	26·0	22·6	—	27·0	32·5	27·0	—	29·0	—	27·2	21·9	28·0	31·6	29·0	26·0	—	—	18
Ba	708	576	745	721	1334	775	788	1262	980	1085	1602	1435	1362	1400	1175	1212	1130	1009	470	1541	580	1346	801	1542	1557	1348	1533	1801	1979	1842
La	86·1	42·4	39·0	40·0	59·9	39·7	39·0	—	—	—	65·3	60·7	48·8	50·8	—	54·7	79·9	63·7	23·9	55·8	35·3	58·0	14·8	54·7	58·5	62·1	47·5	57·7	54·5	33·7
Ce	224	109	121	112	145	99·3	119	152	128	132	130	142	112	119	152	138	180	151	58·0	131	82	132	31	121	130	150	113	137	129	77
Pr	—	—	—	—	—	—	—	—	—	—	19·6	21·4	—	17·7	—	—	26·5	—	—	—	—	19·4	4·91	—	18·8	—	—	—	—	—
Nd	140	72·7	79·0	73·50	—	69·2	73·0	—	—	95·0	92·1	99·0	—	78·6	—	106	119	—	39·0	96·0	52·9	89·5	24·1	—	83·4	108	83·0	87·0	85·0	57
Sm	36·1	20·1	—	19·0	18·9	17·8	—	—	—	—	21·7	22·4	14·1	18·9	—	20·4	27·7	16·9	8·50	17·8	11·5	21·4	6·24	18·8	19·8	16·6	16·2	18·0	17·8	11·7
Eu	8·08	6·82	—	6·80	8·40	6·77	—	—	—	—	7·93	7·55	7·50	7·07	—	7·40	7·31	7·40	2·86	7·70	3·31	7·39	2·83	7·54	6·84	6·50	6·40	6·62	6·77	5·7
Gd	—	—	—	—	—	—	—	—	—	—	18·6	19·6	—	16·0	—	—	26·0	—	—	—	—	25·6	4·53	—	16·0	—	—	—	—	—
Tb	4·21	2·39	—	2·27	2·89	2·15	—	—	—	—	2·69	2·86	2·15	2·26	—	2·40	3·72	2·58	1·13	2·43	1·59	2·73	0·99	2·37	2·50	2·41	2·11	2·46	2·50	1·68
Dy	—	—	—	—	—	—	—	—	—	—	12·5	13·3	—	10·9	—	—	18·8	—	—	—	—	13·2	4·95	—	12·1	—	—	—	—	—
Ho	—	—	—	—	—	—	—	—	—	—	2·34	2·50	—	2·12	—	—	4·04	—	—	—	—	2·49	1·15	—	2·35	—	—	—	—	—
Er	—	—	—	—	—	—	—	—	—	—	5·19	5·53	—	4·63	—	—	9·84	—	—	—	—	5·80	2·85	—	5·79	—	—	—	—	—
Tm	—	—	—	—	—	—	—	—	—	—	0·65	0·69	—	0·59	—	—	1·28	—	—	—	—	0·78	0·46	—	0·74	—	—	—	—	—
Yb	7·43	2·78	—	2·63	4·20	2·48	—	—	—	—	3·49	4·04	3·60	3·33	—	3·80	8·05	4·80	2·00	4·30	3·55	4·38	2·89	4·81	4·21	4·50	3·90	4·70	5·50	4
Lu	1·11	0·43	—	0·39	—	0·35	—	—	—	—	0·48	0·51	—	0·43	—	—	1·16	—	0·33	0·77	0·52	0·56	0·43	—	0·59	0·92	—	0·69	0·85	—
Hf	8·94	2·57	—	2·78	—	2·99	—	—	—	—	5·20	4·40	—	6·91	—	11·0	9·58	5·40	6·50	16·2	7·30	8·80	5·50	12·2	12·1	15·5	17·3	22·10	28·5	32·5
Ta	2·86	1·05	—	1·16	—	1·27	—	—	—	—	1·71	2·23	—	1·04	—	1·68	1·32	1·82	1·31	1·67	1·22	2·05	0·77	1·75	1·50	1·90	1·27	1·89	1·62	0·94
Pb	—	—	—	—	—	—	—	—	—	—	8·55	7·97	—	7·05	—	—	8·72	—	—	20·0	—	11·0	8·08	10·0	12·1	—	—	—	—	—
Th	0·59	0·71	—	0·60	—	0·48	—	—	—	—	<	<	—	<	—	0·79	1·19	1·15	0·50	0·66	3·60	0·23	<	0·67	0·29	0·75	0·59	0·67	0·87	0·66
U	0·17	0·31	—	0·30	—	0·28	—	—	—	—	<	<	—	<	—	0·32	<	—	< 0·2	0·23	1·19	<	<	0·37	<	0·22	0·18	0·10	0·10	0·20
K/Rb	1323	1465	2019	1582	1680	1456	1556	1410	1625	1586	1401	993	1410	1121	1156	1108	747	895	443	1114	376	717	1535	1310	759	822	877	920	733	586
K/Ba	12	13	10	12	11	13	11	12	12	13	9	9	11	10	13	15	11	18	17	18	28	15	11	16	18	24	19	17	18	28
Zr/Hf	45	22	—	20	—	28	—	—	—	—	49	46	—	58	—	40	53	46	40	42	41	54	44	49	51	40	41	—	44	43
Nb/Ta	—	—	—	—	—	—	—	—	—	—	23·3	19·5	—	21·8	—	16·0	24·7	14·8	—	17·4	—	13·3	28·5	16·0	21·0	15·3	20·0	—	—	19
$(La/Yb)_N$	8	11	—	11	10	11	—	—	—	—	13	11	10	11	—	9	7	10	9	9	7	9	4	8	10	10	7	9	7	5
Eu/Eu*	0·72	1·08	—	1·1	0·6	1·21	—	—	—	—	1·15	1·06	1·60	1·19	—	1·15	0·82	0·61	1·05	1·34	0·89	1·08	1·35	1·26	1·09	1·19	1·22	1·14	1·17	1·47

Major elements, Sr and Zn by X-ray fluorescence (XRF), Ni and Cr by instrumental neutron activation analysis (INAA) (analyst J. L. Joron) and others by inductively coupled plasma-mass spectrometry (ICP-MS). In samples 8034 and 7838, trace elements have been analyzed by INAA (analyst J. L. Joron), whereas in samples 66175, 7533, 7534 and 7536, most trace elements have been analyzed by INAA (analyst J. L. Joron), except Ba, Rb, Sr, Zr, Y, V and Zn (XRF; analyst G. Bologne). In samples 7519, 78201, 75182 and 7912, all elements analyzed by XRF (analyst G. Bologne); in sample 75202G, major elements, Zr, Rb, Sr, Ba, Sc, V, Co, Zn and Y by XRF (analyst G. Bologne), and Th, Hf, Ta, Cr and REE by INAA (analyst J. L. Joron); in sample 75206, major elements and Zr, Rb, Sr, Ba, V, Cr, Zn, Nb and Y analyzed by XRF (analyst G. Bologne), and Th, Hf, Ta, Sc, Co, Ni and REE by INAA (analyst J. L. Joron). P is the average of samples 66175, 7533, 7534 and 7536. —, not analyzed; <, below detection limit. †Wilmart (1988): major elements and Rb, Sr, Ba, Y, Zr, V and Zn by XRF; others by INAA. ‡Duchesne & Hertogen (1988): major elements and Rb, Sr, Ba, Y, Zr, V and Zn by XRF; others by INAA. §Duchesne *et al.* (1974): major elements and Rb, Sr and Zr by XRF; other trace elements by INAA.

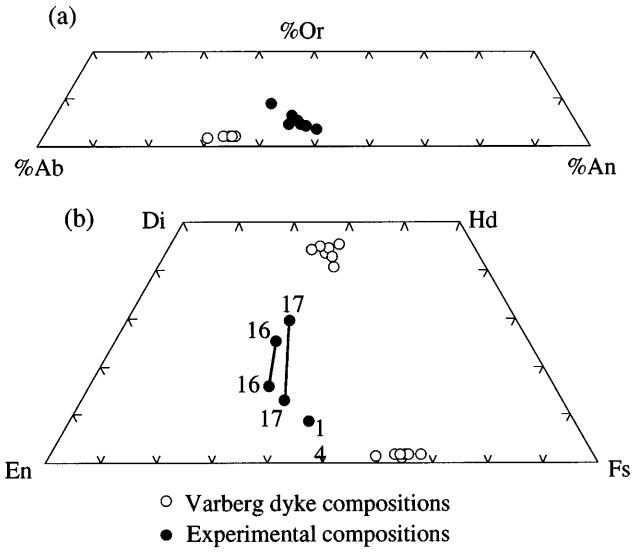

Fig. 3. Anorthite content of plagioclase (a) and pyroxene compositions (b) [En ($MgSiO_3$)–Fs ($FeSiO_3$)–Di ($CaMgSi_2O_6$)–Hd ($CaFeSi_2O_6$) quadrilateral] in the Varberg dike (Table 4) as well as in liquidus and near-liquidus experiments (VB runs) (Table 3). Numbers in the pyroxene quadrilateral are run numbers.

charge. The few areas of glass are chemically heterogeneous (Table 3), and thus represent local surface equilibrium. Mass balance calculations show that there is a precipitous drop in percent liquid between 1080°C (82%) and 1078°C (61%), so encountering the solidus a few degrees lower is not surprising; however, in VB-5 at 1060°C, which should have been below the solidus, a small amount of glass with 67·6% SiO_2 was observed adjacent to K-feldspar. An explanation of these phenomena can be deduced from Fig. 4, in which liquidus phase diagrams are drawn from experimental phase compositions. In a plagioclase–ilmenite–apatite projection (Fig. 4a), the compositions of liquid, pigeonite, and olivine (plus plagioclase, ilmenite, and apatite) in VB-14 are nearly coplanar, implying a thermal divide on the olivine–pigeonite (+ plagioclase, ilmenite, and apatite) liquidus boundary, which in turn promotes extensive crystallization in a narrow temperature interval. Moreover, both the plagioclase–ilmenite–apatite projection (Fig. 4a) and the wollastonite–ilmenite–apatite projection (Fig. 4b) indicate that the VB-14 liquid composition is also close to a second thermal divide plagioclase–pigeonite (+ augite, apatite, and ilmenite) and a eutectic olivine + plagioclase + pigeonite (+ augite + apatite + ilmenite). This latter thermal divide restricts SiO_2 enrichment at 5 kbar and low $f(O_2)$ and prevents olivine-saturated liquids from ever reaching quartz saturation. Had magnetite been stable or the pressure lower, it is likely that the eutectic would become a peritectic (olivine in reaction) and that liquids would be able to breach the augite–pigeonite thermal divide. Given the absence of magnetite in the various runs and the array of phase relations in Fig. 4, we believe that the high-SiO_2 glass in VB-5 is primarily the result of local equilibrium in the experimental charge where more mafic domains having a higher solidus temperature remained entirely crystalline, whereas more felsic domains having a lower solidus temperature yielded a small amount of high-SiO_2 melt. Therefore, as with VB-13, even though run VB-5 did not achieve bulk equilibrium, the liquid is probably multiply saturated nonetheless, so we have used the VB-5 glass composition to approximate the multiple saturation surface of charnockitic (high-SiO_2) liquids. A second curious point is the apparent absence of olivine in VB-14, despite the fact that olivine is present in runs immediately above (VB-4) and below (VB-13) this temperature. Given that the composition of the olivine + plagioclase + pigeonite (+ augite, apatite, and ilmenite) pseudo-invariant point lies close to a line from the Pl component through the VB composition, it is likely that a small difference in pressure between the two runs produced a different crystallization sequence: lower pressure in VB-4 (ol, no pyx) shifted the pseudo-invariant point away from the Ol component and stabilized olivine; whereas higher pressure in VB-14 shifted the pseudo-invariant point toward the Ol component and stabilized low-Ca pyroxene. Accordingly, olivine should be stable at the same pressure as, but at a lower temperature than VB-14, which is what is observed in VB-13.

At 1 atm and the NNO buffer, pigeonite, augite, plagioclase, and phosphate are stable together near the solidus with the only Fe–Ti oxide being titanomagnetite (actually ferri-ulvöspinel: $uvsp_{58}mgt_{42}$ in VB-16), whereas

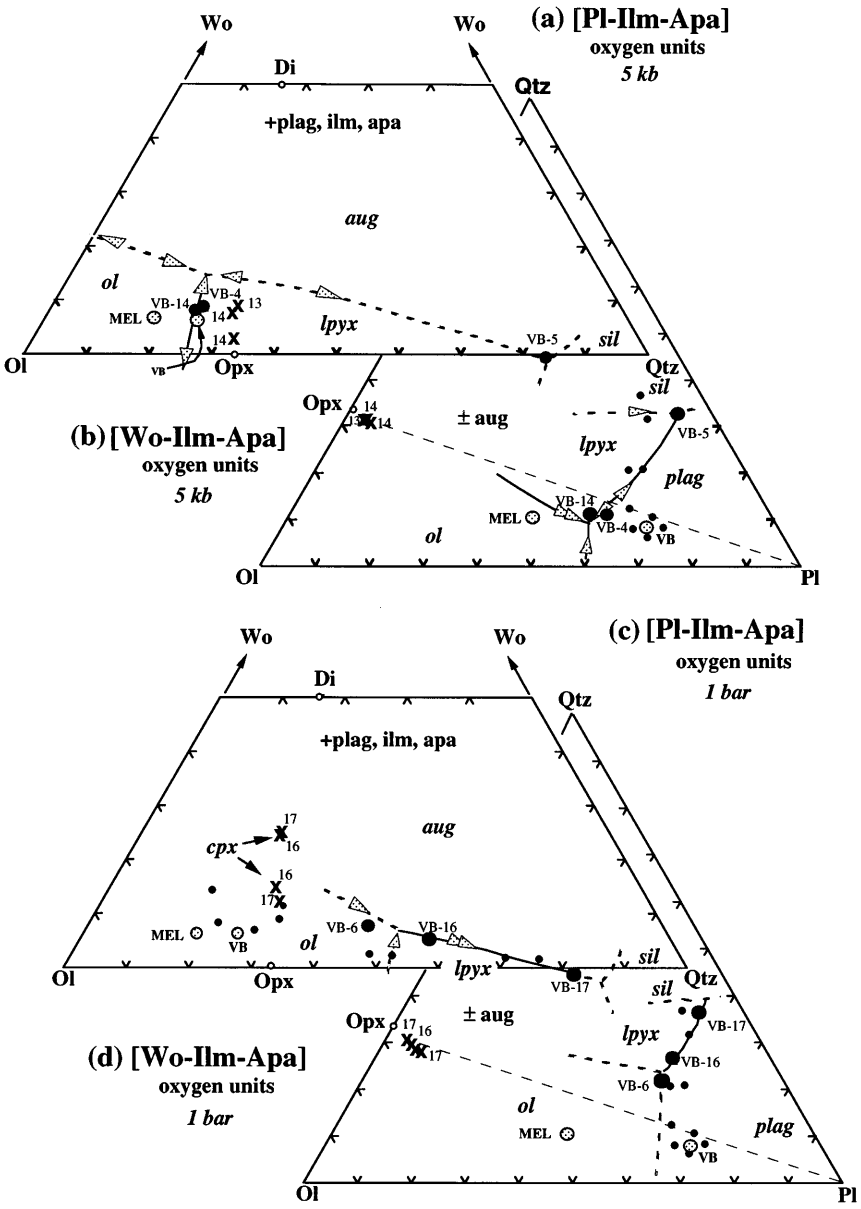

Fig. 4. Projections according to Longhi (1991) on the silica–olivine–wollastonite plane from plagioclase, ilmenite and apatite and on the silica–olivine–plagioclase plane from wollastonite, ilmenite and apatite. In (a) and (b), 5 kbar experiments are shown; in (c) and (d), 1 bar experiments. In all diagrams except (a), the small black dots correspond to the fine-grained samples and the large stippled points to starting compositions (VB and MEL). Low-Ca pyroxene (lpyx) composition (×) are from VB-13 and VB-14 in (a) and (b) and from VB-16 and VB-17 in (c) and (d). In (a) and (b), VB-4 and VB-14 glasses (●) were used to position the ol + plag + lpyx boundary and the VB-5 glass provides some constraint on the sil + lpyx + plag (+ aug) point. In (c) and (d), the ol + plag + lpyx boundary has been constrained with the VB-6 (●) and VB-16 (●) glasses whereas the VB-17 glass fixes the plag + lpyx + aug boundary.

at the FMQ buffer, both ilmenite and ferri-ulvöspinel ($uvsp_{69}mgt_{31}$ in VB-6) precipitate (Table 2). We presume that olivine would be stable at higher temperatures at NNO, as it is at FMQ. Phosphate analyses (Table 3) indicate that fluorine is present in the 5 kbar experiments but not in the 1 atm experiments, suggesting that the phosphate is probably fluoroapatite in the former and whitlockite in the latter. The liquidus boundaries drawn on the basis of the 1 atm experiments are shown in Fig. 4c and d. They indicate that under moderately oxidizing

low-pressure conditions the thermal divide involving augite + low-Ca pyroxene + plagioclase is not stable and that olivine is in reaction with liquid when low-Ca pyroxene is stable. Thus olivine, which is the first mafic phase to crystallize in the jotunite compositions at low pressure, will be replaced by low-Ca pyroxene and plagioclase (Fig. 4d) at a peritectic reaction, and further fractional crystallization will drive the liquid toward silica saturation, and produce SiO_2 enrichment. The liquidus topology is consistent with petrological variations observed in the Tellnes orebody and its associated dike (Wilmart *et al.*, 1989) where olivine-bearing ilmenite norite contains the minerals with the most primitive compositions, and other lithologies are olivine free and grade continuously from jotunite to mangerite to quartz mangerite.

Titanomagnetite is present together with ilmenite in the matrix of the Varberg dike; however, both oxides have been exsolved and subjected to strong subsolidus reequilibration (Duchesne, 1972*a*), so their compositions provide no constraint on redox conditions in the dike. Accordingly, we have estimated redox conditions in the dike on the basis of experimental Fe–Ti oxide assemblages. At 1 atm and the FMQ buffer, two Fe–Ti oxides are stable, $ilm_{86}hem_{14}$ and $uvsp_{69}mgt_{31}$, whereas at 1 atm and the NNO buffer, only spinel precipitates ($uvsp_{58}mgt_{42}$ in VB-16; $uvsp_{48}mgt_{52}$ in VB-17). Also, previous work on a primitive jotunite has shown that FMQ – 1 marks the low-$f(O_2)$ stability limit for spinel in these compositions (Vander Auwera & Longhi, 1994). Thus, inasmuch as both spinel (magnetite) and ilmenite are present in the dike, the $f(O_2)$ was probably close to the FMQ buffer during crystallization.

Natural and experimental pyroxene compositions have been plotted in a Al_2O_3 vs CaO diagram (Fig. 5) in an attempt to glean some information about the pressure of crystallization of the dike. The situation is complicated by inversion and exsolution in the pyroxene; however, the primary pyroxene compositions are constrained to lie on mixing lines between host and lamellae. Both the 1 atm and 5 kbar data fall above (higher Al_2O_3) the mixing lines of the natural pyroxenes in Fig. 5, indicating no simple relationship. Comparison of pyroxene compositions in the two 5 kbar runs suggests that the lower Al_2O_3 content observed in the natural pyroxenes may result from continued equilibration to the solidus and into the subsolidus. Even so, there is no way to discriminate between 1 atm and 5 kbar on the basis of Al_2O_3 concentrations. However, the experimental data suggest that CaO decreases systematically with increasing pressure. Consequently, we have calculated the CaO concentration of the primary pigeonite from the compositions of orthopyroxenes and exsolved augites in samples 78201 and 75202G (Table 4) and the modal proportions of orthopyroxene hosts and augite exsolutions (optical determination). The range of calculated compositions of natural pyroxenes (4·8–5·9 wt % CaO) is slightly higher than the value calculated by Duchesne (1972*b*) for inverted pigeonites from BKSK (3·7–4·7% CaO). The values indicate a pressure of emplacement between 1 atm and 5 kbar (Fig. 5), the latter pressure being consistent with estimates for the crystallization of the Bjerkreim–Sokndal intrusion (Vander Auwera & Longhi, 1994).

Because the chill margin composition (VB) projects well into the plagioclase field in Fig. 4b and d, it is clear that the chill margin is not itself a quenched liquid at pressures of 5 kbar or less. In the 5 kbar near-liquidus run, VB-2, plagioclase has the composition An_{46}, whereas the most anorthitic plagioclase in the chill margin sample is only An_{36}. So the chill margin is not even a simple quenched liquid. In Fig. 4b (5 kbar) the chill margin lies nearly on a line between the plagioclase component and the pseudo-invariant point. These relations, together with the abrupt simultaneous appearance of olivine, ilmenite, and apatite in the crystallization sequence, are consistent with the chilled margin being a multi-saturated liquid, like VB-4 or -14, enriched with 15–30% plagioclase by weight. It should be noted that plagioclase in run VB-14 has an average composition of An_{38}, which is close to that observed in the dike, and which supports a multi-saturated liquid composition similar to that of VB-14. Alternatively, if the jotunite magma was derived by fractionation at a higher pressure where multi-saturated liquids sustain higher plagioclase components (Vander Auwera & Longhi, 1994), some portion of the apparent excess plagioclase component would be due to decompression, and the actual liquid composition would be displaced toward the Pl component, but not as far as the chill margin composition (Vander Auwera & Longhi, 1994). So, despite the fine grain size of the chill margin and the absence of phenocrysts, the material flowing along the margins of the dikes contained some plagioclase crystals in suspension. The more evolved compositions of the fine-grained samples with higher Qtz components do fall close to the plagioclase + pyroxene cotectics in Fig. 4b and d, so it is likely that the more evolved fine-grained samples within the dikes closely approximate liquid compositions.

Whole-rock analyses

The fine-grained samples from the Varberg dike and various other dikes display high total Fe as FeO_t (9·65–16·03%),TiO_2 (1·27% up to 4·62%), K_2O (0·96% up to 4·24%), and P_2O_5 (0·71% up to 2·59%) concentrations together with a modest range in SiO_2 (46·45% up to 60·41%) (Table 5, Fig. 2). In variation diagrams (Fig. 2), the primitive jotunites form a group distinct from the

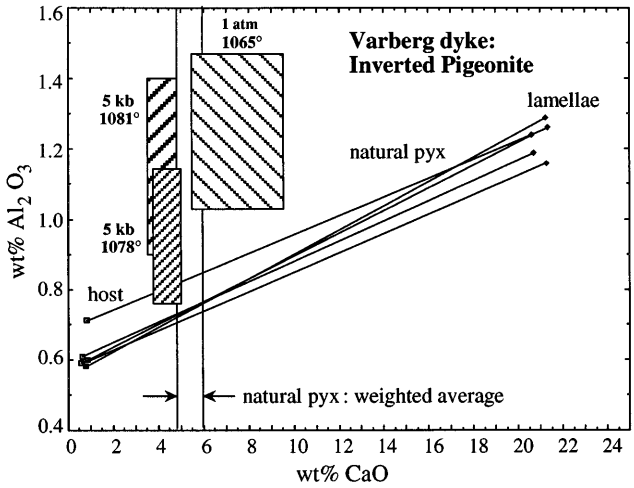

Fig. 5. Al_2O_3 and CaO contents of natural and experimentally obtained pyroxenes. For the experimental compositions, boxes correspond to 1 SD. The calculated compositions of natural pyroxenes correspond to their compositions before exsolution (see text for explanation).

jotunites of the dike system, which define trends of decreasing FeO_t, TiO_2, P_2O_5 and CaO, and increasing SiO_2 and K_2O, with decreasing MgO. Samples of jotunites from other localities have been included in Fig. 2 for comparison. Among them, two [sample 738: Owens *et al.* (1993); sample EC90-216: Emslie *et al.* (1994)] are very similar to the primitive jotunites of Rogaland whereas the others fall near or on the trend of the dike system. Nevertheless, a group of samples from Nain (Wiebe, 1979) and Grenville (Owens *et al.*, 1993) define a trend higher in CaO/MgO and lower in K_2O/MgO than samples from the other localities. This probably results mainly from different fractionation paths from locality to locality (see discussion) and from accumulation of plagioclase + mafics. This latter process can also explain the dispersion observed in samples from the Laramie complex (Mitchell *et al.*, 1996) especially in the FeO_t/MgO, TiO_2/MgO and P_2O_5/MgO diagrams.

La concentrations in the fine-grained samples and other representative samples range from 15 ppm to 80 ppm (Table 5). The evolved jotunites, mangerites and quartz mangerites (Fig. 6) are higher in total REE content than the primitive jotunites, except the quartz mangerite 7832 which is in the range of primitive jotunites. The fine-grained samples display similar light REE (LREE) enrichment [average $(La/Yb)_N = 9$] except for one sample [91141: $(La/Yb)_N = 4$]. Eu anomalies are either weak—slightly negative or slightly positive (e.g. 91141)—or absent.

In a multielement diagram (Fig. 7), the primitive jotunites display variable concentrations of several trace elements, especially for Th, Rb, and REE (see also U in Table 5), whereas their major element concentrations are rather constant except for K. Duchesne *et al.* (1989) previously pointed out this feature and attributed it to the variability of the source of jotunites. Apart from the enormous variation in Th, the primitive jotunites have relatively featureless patterns in contrast to the highly fractionated patterns of the evolved jotunites, mangerites and quartz mangerites. Primitive jotunites show small depletions of Ta (not Nb) and Hf (but not Zr in all cases) relative to the adjacent REE, whereas Ti shows a small excess as does P. Also, Sr may show a small depletion (80123a, 7234 in Fig. 7), where Eu shows no depletion (Fig. 6), or Sr may show no depletion (91141) where Eu shows a small excess. However, all the evolved jotunites, mangerites and quartz mangerites show prominent depletions in Sr relative to Ce and Nd, yet Eu anomalies remain small and may even be positive in the quartz mangerites. The Sr depletions indicate extensive crystallization of plagioclase despite the evidence for plagioclase accumulation in some samples. The unexpected behavior of Eu is discussed below. Interestingly, P, which shows small relative excesses in the primitive jotunites, shows larger excesses in the evolved jotunites and then little or no excess or depletion in the mangerites, and finally prominent depletions in the quartz mangerites. This pattern signals the onset of apatite crystallization as the magma changes from jotunitic to mangeritic. Relative depletions of Nb–Ta become more pronounced, and pronounced relative depletions of Ti develop with differentiation, whereas relative depletions of Hf and Zr diminish in the mangerites and even become slight enrichments in the quartz mangerites, which are consistent with Ti-oxide crystallization, but not zircon. Th shows huge depletions relative to the LREE in all of the evolved

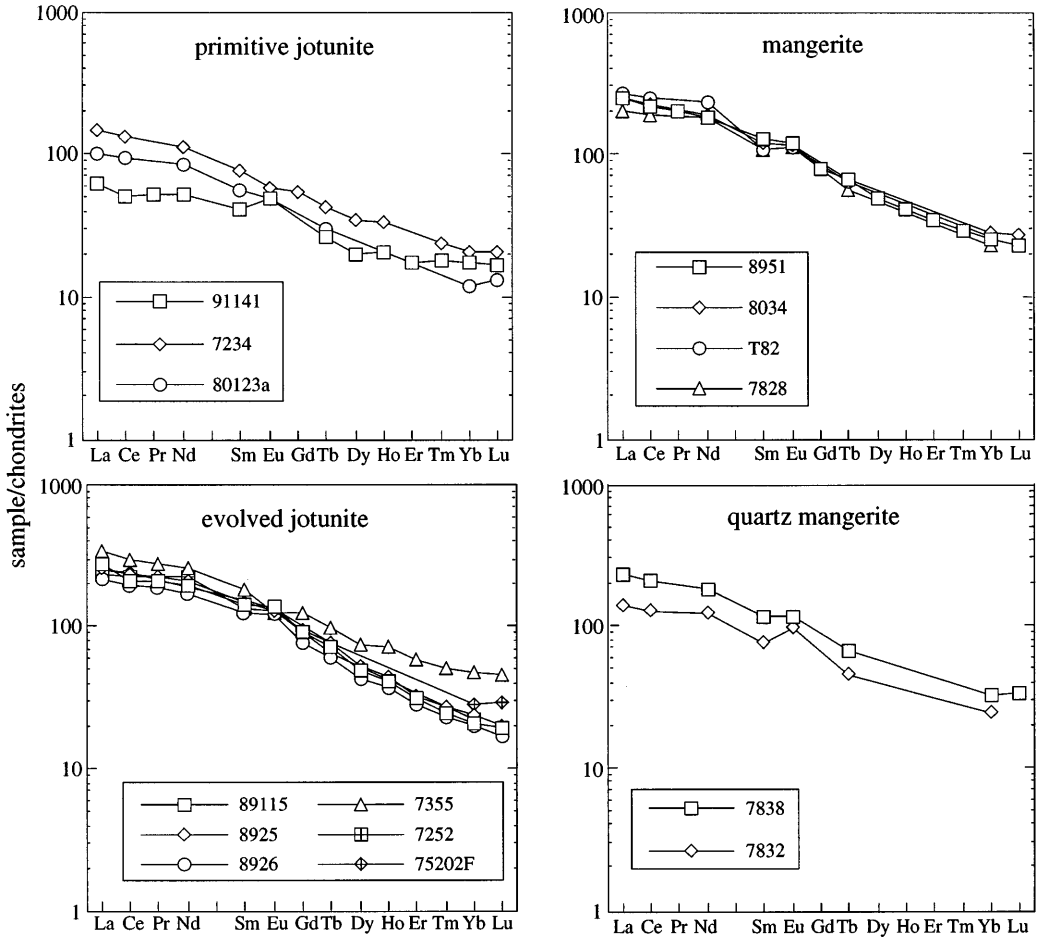

Fig. 6. REE patterns of the jotunitic suite [7234 (Duchesne *et al.*, 1974); 80123a (Duchesne & Hertogen, 1988); 7252, 7828, T82, 7832 (Wilmart *et al.*, 1989)]. REE abundances normalized to C1 chondrite of Sun & McDonough (1989).

jotunites despite its variability in the primitive jotunites, suggesting that the Th–REE relation is a characteristic of the parental magma, and of the three primitive jotunites only 80123a could be parental to the evolved jotunites. Primitive jotunites also show considerable range in K_2O with limited variation in MgO (Figs 2 and 8). These features suggest variable contamination of the large intrusions by country rock gneisses during emplacement (Hoover, 1989; Wilson *et al.*, 1996). For all the samples the K/Rb ratio varies from 376 to 1535 and Zr/Hf from 40 to 58. These trace elements compositions are in the range of those previously reported by Duchesne (1990) for the jotunitic suite of the Rogaland Province and are similar to those reported in other anorthositic complexes [e.g. Grenville Province: Emslie *et al.* (1994); Laramie Complex: Kolker *et al.* (1990); Mitchell *et al.* (1996)].

A LIQUID LINE OF DESCENT OF THE JOTUNITE SUITE AND ORIGIN OF ROCKS WITH EXTREME Fe–Ti–P CONTENT

Liquid line of descent (LLD)

A series of samples presented in this study display petrographic features typical of chilled rocks that suggest they are close to liquid compositions and thus constrain a liquid line of descent of the jotunitic suite under dry conditions. Nevertheless, projection of the fine-grained samples in the Ol–Pl–Qtz diagram (Fig. 4) seems to indicate that some of them are enriched in plagioclase. We have already mentioned that the fine-grained samples define in variation diagrams (Fig. 2) two clusters of

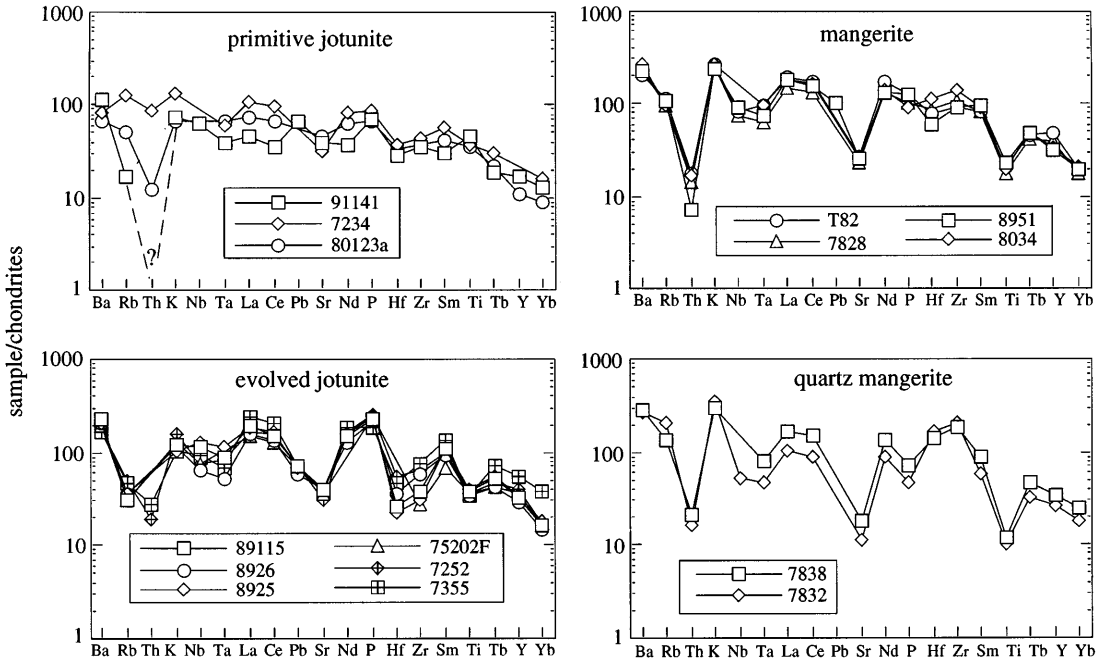

Fig. 7. Multielement diagrams of the jotunitic suite [7234 (Duchesne *et al.*, 1974); 80123a (Duchesne & Hertogen, 1988); 7252, 7828, T82, 7832 (Wilmart *et al.*, 1989)]. Abundances normalized to chondrites (Thompson, 1982).

points, one with a narrow range of intermediate MgO, corresponding to the primitive jotunites (chilled margins of large intrusions), and the other, offset from the first, forming linear trends ranging from evolved jotunites to quartz mangerites, in which FeO_t, TiO_2, and CaO decrease, whereas K_2O and SiO_2 increase, versus decreasing MgO. These trends are repeated by samples from other dikes in the Rogaland system. The compositions of samples from the Tellnes dike, for example, overlap those from the Varberg dike and extend the trend to higher SiO_2 (charnockite). Thus in Rogaland there is an apparent discontinuity between primitive jotunite and evolved jotunite, but continuous chemical variation from evolved jotunite, through quartz mangerite, to charnockite.

The experimental data obtained on the two Varberg dike samples plus previous data on the Tjørn jotunite (Vander Auwera & Longhi, 1994), which belongs to the group of primitive jotunites, bring additional constraints on the LLD. However, some care must be taken because the compositions of the experimental liquids vary by equilibrium crystallization, whereas the jotunite LLD more probably results from a partially fractional crystallization process, and also because the pressure–redox conditions of the experiments do not match those of the dikes. Delayed crystallization of ilmenite, the absence of magnetite near the solidus, and decreased *mg*-number of ferromagnesian phases all are effects of the low Fe^{3+}/Fe^{2+} ratio imposed by the graphite capsules; and even though the 1 atm experiments have been run at the appropriate $f(O_2)$, the lower pressure increases the proportion of plagioclase and olivine crystallization relative to pyroxene. These difficulties turn out to be relatively minor if one compares a combination of the 1 atm and high-pressure (5 and 7 kbar) data with the variation pattern of the dikes, as illustrated in Fig. 8, where the shaded areas correspond to the compositional ranges of the Rogaland jotunites shown in Fig. 2.

The most important feature is that the FMQ VB point (run VB-6) lies on or very near the dike trend in all of the panels (Fig. 8). The track of NNO VB is parallel to the dike trend, but is offset from the dikes in the direction of higher SiO_2 and lower FeO_t and TiO_2, because of the crystallization of too high a proportion of Fe–Ti-oxides. The track of 5 kbar VB follows a path of much higher FeO_t and lower SiO_2 than the dikes, as the reducing conditions imposed by the graphite capsules delay the crystallization of Fe–Ti oxides, which in turn induces an excessive ferrous iron content in the liquid. It thus seems likely that crystallization of a liquid with VB-like composition at modest pressures and with $f(O_2)$ close to FMQ would produce a track very close to the dike trend, and that following eventual crystallization of titanomagnetite the track would extend to high SiO_2 (charnockitic) concentrations.

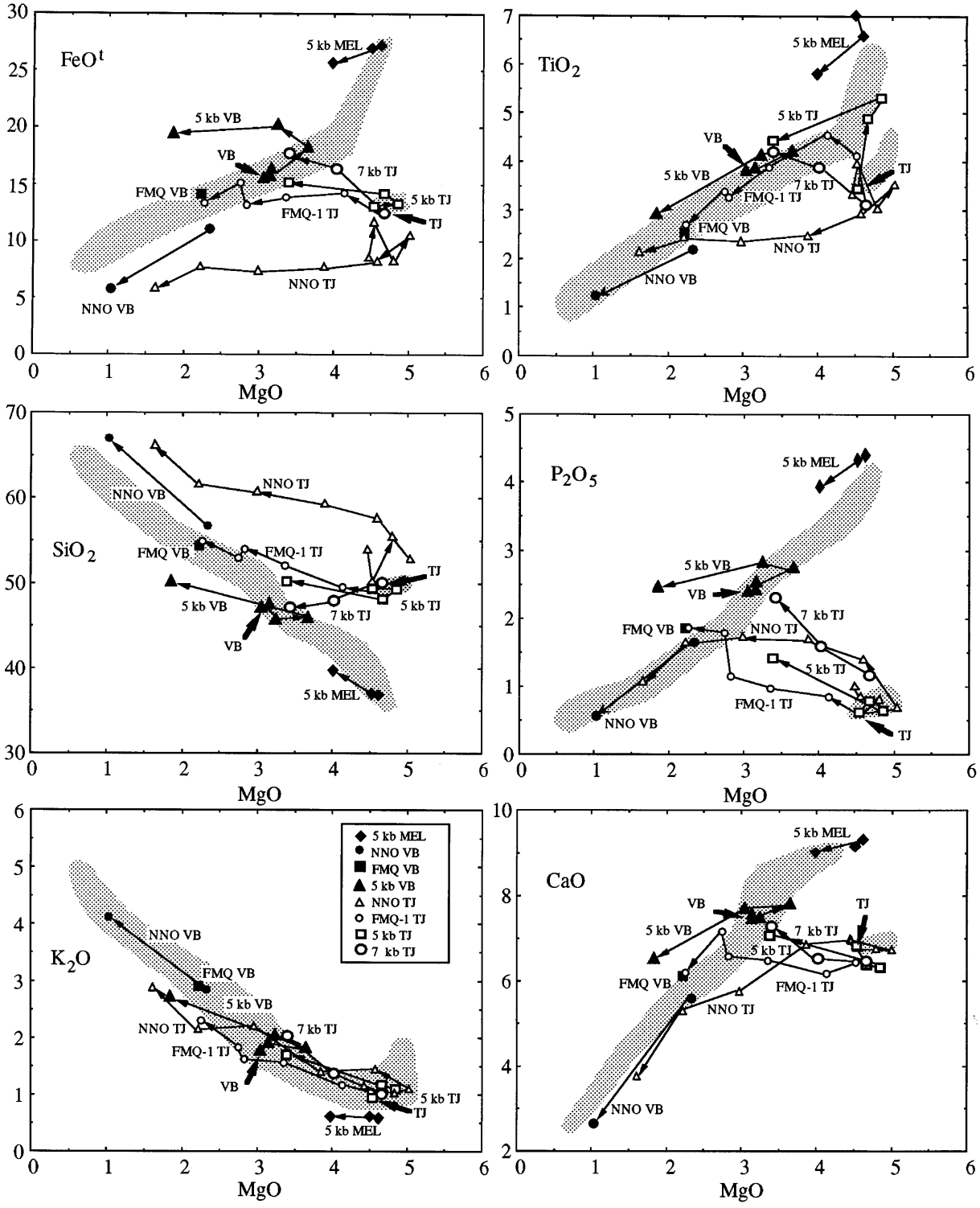

Fig. 8. Comparison of experimental data (wt % oxides) on VB (75202F), MEL (75372), and TJ (Vander Auwera & Longhi, 1994) with the Rogaland jotunitic trend from Fig. 2 (shaded areas).

Comparison of the data on a primitive jotunite (TJ) from a previous study (Vander Auwera & Longhi, 1994) with data on the evolved jotunite (VB) from the present study provides further constraints on their possible relationship. In all sets of experiments on TJ, TiO_2 and FeO_t increase with decreasing temperature until ilmenite becomes a liquidus phase. While plagioclase is the sole crystallizing phase, the initial TiO_2 and FeO_t tracks show an increase with decreasing temperature. The effect of ilmenite saturation is probably best illustrated by the TJ experiments run at 1 atm (FMQ – 1 TJ). In this case, the maximum TiO_2 concentration (~4·5 wt %) is reached at ~4 wt % MgO. As temperature decreases further, TiO_2 and FeO_t decrease with MgO, whereas SiO_2 increases. The tracks of TiO_2, FeO_t, and SiO_2 for FMQ – 1 TJ eventually all join the trend of the dike compositions: FeO_t and SiO_2 at MgO lower than that of sample VB; TiO_2 at MgO higher than VB. Crystallization of TJ at higher pressure will move the tracks of the FeO_t and SiO_2 closer to VB. If titanomagnetite were to crystallize after ilmenite at 5 kbar, the 5 kbar tracks of both VB and TJ would move closer to and follow the dike trend. P_2O_5 concentration in the liquid increases with decreasing temperature until phosphate crystallizes in experiments on both TJ and VB. In the VB experiments, apatite begins to crystallize simultaneously with ilmenite and olivine (VB-4): this liquid is probably very close to the Varberg liquid composition (see above). The TJ data also show that the early increase in P_2O_5 appears more pronounced at high pressure. This pressure effect derives from a greater proportion of pyroxene crystallizing relative to olivine at higher pressure: olivine can incorporate a small amount of P_2O_5 [more than low-Ca pyroxene: see Vander Auwera & Longhi (1994)] and Mg decreases more rapidly because of the higher Mg content of olivine. SiO_2 decreases with temperature in TJ liquids at 7 kbar because of co-crystallization of high-Si plagioclase and orthopyroxene and a low proportion of ilmenite; whereas at 5 kbar SiO_2 increases weakly because olivine is the sole mafic–silicate phase near the liquidus. K_2O always increases and the residual experimental TJ liquids reach the K_2O content observed in dikes.

An important feature of Fig. 8 is thus the bridge made between the field of primitive jotunites and the trend of evolved jotunites by liquids residual to TJ. At 5–7 kbar the paths of the TJ liquids join the evolved jotunite trend close to the multi-saturated VB experimental liquids that most closely approximate the parental liquid of the Varberg dike. Consequently, the apparent discontinuity between primitive and evolved jotunites shown in Fig. 2 could result from a lack of exposures of this early fractionation stage. This process probably took place below the intrusion level of the dikes.

Origin of the extreme concentrations of Fe, Ti and P in some jotunites

Jotunites characterized by very high concentrations of FeO, TiO_2 and P_2O_5 (FTP) have been recognized in all anorthosite complexes (Ashwal, 1982; Owens & Dymek, 1992; Owens *et al.*, 1993; McLelland *et al.*, 1994). Emslie *et al.* (1994) and McLelland *et al.* (1994) have proposed that the unusually high Fe–Ti–P content is characteristic of a liquid derived from the processes of anorthosite crystallization under reducing conditions. FTP-rich jotunites from Rogaland have been recognized in the Varberg and Lomland dikes. In the latter, they constitute the Puntervoll facies, which passes progressively along strike into jotunites, mangerites and quartz mangerites. An average of four analyses of the Puntervoll facies (Duchesne *et al.*, 1985) plots on an extension of the trend of evolved jotunites at 3·9 wt % MgO ('P' in Fig. 2). In the Varberg dike, the transition between the FTP rocks and the common jotunites is not observed in the field but these FTP rocks (e.g. MEL with 4·20% P_2O_5, 6·23% TiO_2 and 27·43% FeO_t) plot with higher FeO and TiO_2 than simple extensions of the dike trend (Figs 2 and 8). The chemical variation toward low-SiO_2 compositions is more nearly continuous in anorthosite complexes from the Grenville Province (Owens & Dymek, 1992; McLelland *et al.*, 1994).

Variation diagrams combining experimental and geochemical data (Fig. 8) indicate that the composition of sample MEL cannot be simply explained by fractionation from a primitive jotunite even under very reducing conditions [$f(O_2)$ in the 5 and 7 kbar TJ experiments lies between FMQ – 2 and FMQ – 4]. Consequently, given that field evidence indicates that sample MEL is comagmatic with VB, three alternatives are left: the FTP-rich jotunites may correspond to immiscible liquids conjugate to the mangerites found in the same dikes (e.g. Lomland) or they can represent liquids more or less heavily laden with Fe–Ti oxides and apatite or possibly cumulates injected as a crystal mush (Ashwal, 1982).

The position of sample VB in the jotunitic differentiation trend corresponds to the culmination of FeO_t and TiO_2 concentrations in the jotunite trend and thus it is the most likely candidate to plot within the immiscibility field (Roedder, 1979). However, the experimental MEL liquid compositions (Fig. 8) trend toward the array of evolved jotunite compositions with decreasing temperature, i.e. SiO_2 and K_2O increase as MgO, FeO, P_2O_5, and TiO_2 decrease. Therefore the VB and MEL compositions are not situated on opposite sides of some immiscibility field. There is also no evidence (globules, menisci) of two liquids of any kind (silicate–silicate or silicate–oxide) in any of the experiments. Plagioclase is not a near-liquidus phase of the MEL composition, nor is there any textural or petrographic evidence for

immiscibility in the dike itself. Moreover, if we assume that, in the Varberg dike, the melanorite represented by sample MEL and the mangeritic composition represented by the Kungland facies (Duchesne *et al.*, 1985) correspond to conjugate immiscible liquids, the partition coefficients of P, Zr, REE, Ba and Sr are much lower than those measured by Watson (1976). We therefore conclude that immiscibility is not a relevant process for the formation of the FTP rocks, which leaves crystal accumulation (perhaps achieved through flow differentiation) as the only viable mechanism to produce FTP rocks.

Given that plagioclase is texturally primitive (hypidiomorphic) in the Varberg dike and is ubiquitous in the cumulates (BKSK intrusion), the absence of plagioclase near the liquidus of the melanorite MEL is a clear indication that the rock has accumulated non-felsic minerals. However, experiments performed on the MEL sample show that its liquidus temperature (1110°C) is similar to that of the chilled margin (1120°C) of the Varberg dike, and is only marginally higher than the temperature of the likely parental liquid (~1080°C; VB-14), despite its having higher FeO_t and lower SiO_2. If a rock is a chilled suspension of a single phase in a liquid, the liquidus temperature of the rock will be higher than the temperature at the time of accumulation and the liquidus phase is likely to crystallize over a large temperature interval. However, if several phases have accumulated then there is the possibility of little or no increase in liquidus temperature as in the case of eutectic accumulation. Multi-phase accumulation appears to be the case for the relatively low liquidus temperature of MEL, and the similarity of the liquidus temperatures of VB and MEL is thus partly coincidental. Nevertheless, the situation is more complex here, as only the non-felsic part of the saturating assemblage—ilmenite, magnetite, apatite, and possibly orthopyroxene—appears to have accumulated to form the melanocratic facies. In the projections (Fig. 4), though, there appears to be a displacement of the MEL composition away from liquids saturated with the dike's assemblage not toward orthopyroxene, but toward the olivine component. This disparity may be attributed to Fe^{3+} incorporated in the accumulated Fe–Ti oxides, but treated as Fe^{2+} in the projections. Subtraction of this Fe will drive the projected MEL composition toward Qtz on a line parallel to the Ol–Qtz join, thus increasing the proportion of orthopyroxene relative to olivine in the apparent accumulated component.

Major element modeling

To model the trace element variations in the jotunitic trend, we must first constrain the phase proportions and, hence, the major element variation. In the following, we will present a three-stage model based on previous petrogenetic studies of other Rogaland dikes (Duchesne *et al.*, 1985; Wilmart *et al.*, 1989) as well as of the BKSK layered intrusion (Duchesne, 1978). Stage 1 of the model involves fractionating a primitive jotunite, similar to the parental magma of BKSK (TJ: sample 80123a) to produce an evolved jotunite; the second stage involves fractionating an evolved jotunite, similar to VB to produce a mangeritic composition; and the third stage involves fractionating a mangeritic composition to produce quartz mangerite.

Variation diagrams in Fig. 8 show that subtraction of a leuconoritic assemblage from TJ drives the residual liquid toward the field of evolved jotunite compositions, close to the chilled margin composition of the Varberg dike (VB). In the different sets of experiments on TJ (Vander Auwera & Longhi, 1994), cumulus assemblages in equilibrium with the liquid closest to VB are: 64% plag + 30% low-Ca pyroxene + 6% ilm at 7 kbar, 74% plag + 20% ol + 2% pig + 4% ilm at 5 kbar, and 70% plag + 18% ol + 12% oxides at 1 atm and FMQ − 1. These phase proportions closely match the leuconoritic cumulate deduced by Duchesne (1978) (74% plag + 16% low-Ca pyroxene + 10% ilm) from the Sr–Ca modeling of the leuconoritic stage of BKSK, except that olivine is the major ferromagnesian phase at 5 kbar and 1 atm instead of low-Ca pyroxene. Moreover, the fraction of liquid is 0·47 at 5 kbar and 0·51 at 1 atm, which is close to the value ($f = 0{\cdot}47$) calculated by Duchesne (1978). The phase proportions observed in the experimental cumulates correspond to an equilibrium crystallization process whereas those derived for BKSK are based on a fractional crystallization process. Nevertheless, as a fractional crystallization process is more relevant for the jotunitic trend discussed here, we have chosen a cotectic leuconoritic cumulate made of 74% plag + 16% low-Ca pyroxene + 10% ilm with $f = 0{\cdot}5$ for the first stage.

To further model the fractional crystallization process along the jotunitic trend, there is the possibility to use simulations based either on partition coefficients (Nielsen, 1990) or on minimization of the Gibbs free energy (Ghiorso & Sack, 1995). Nevertheless, it has been shown that these simulations do not predict well the saturation of Fe–Ti oxides (Toplis & Carroll, 1996). We have therefore used mass balance calculations to further model the major element variations in the jotunitic trend. In the case of fractional crystallization, the mineral phase compositions must be in equilibrium with the starting liquid and this will be true for a certain amount of crystallization after which a new set of mineral compositions must be selected. We assume that the parent magma of the Lomland dike was close to the Varberg chilled margin (VB) and to the Eia–Rekefjord chill (7355) but we must point out that these compositions are probably slightly enriched in plagioclase, so that we use parent

Table 6: Three-stage major element model

Calculated cumulates

Primitive jotunite

C1 = 74% plag (An_{43}) +16% low-Ca pyrx + 10% ilm ($f1 = 0{\cdot}5$, $F = 0{\cdot}5$)

Evolved jotunite

C2 = 43·3% plag + 19·6% low-Ca pyrx + 8·5% high-Ca pyrx + 9·3% ilm + 11·3% mgt + 8% ap ($f2 = 0{\cdot}6$, $F = 0{\cdot}3$)

Mangerite

C3 = 46·9% plag + 11·3% low-Ca pyrx + 12·7% high-Ca pyrx + 2·8% ilm + 21·1% mgt + 5·2% ap ($f3 = 0{\cdot}67$, $F = 0{\cdot}2$)

Least-squares fractionation model for cumulate 2 (C2)

				Mineral compositions used in fit					
	Evolved jotunite*	Mangerite	Cumulate	Plag (An_{40})	Opx (*mg*-no. 0·56)	Cpx (*mg*-no. 0·66)	Ilm (Hem_2)	Mgt ($Uvsp_{15}$)	Apa
SiO_2	47·30	51·60	40·55	58·52	50·38	51·22	0·49	1·74	0·00
TiO_2	3·55	2·41	5·25	0·00	0·14	0·42	48·81	4·84	0·00
Al_2O_3	13·70	14·65	12·42	26·31	1·22	2·12	0·39	3·10	0·00
FeO_t	15·83	13·28	19·48	0·00	25·90	11·53	44·71	78·98	0·00
MgO	3·20	2·26	4·90	0·00	18·62	12·44	0·55	0·46	0·00
MnO	0·25	0·19	0·29	0·00	0·00	0·00	0·00	0·00	0·00
CaO	7·65	6·21	9·86	7·86	0·74	20·34	0·10	0·11	54·80
Na_2O	3·56	3·96	2·95	6·50	0·13	0·65	0·00	0·00	0·00
K_2O	1·70	3·00	0·35	0·80	0·00	0·00	0·00	0·00	0·00
P_2O_5	2·27	1·44	3·40	0·00	0·00	0·00	0·00	0·00	41·70
$\Sigma r^2 = 0{\cdot}086$									

Least-squares fractionation model for cumulate 3 (C3)

				Mineral compositions used in fit					
	Mangerite†	Quartz mangerite	Cumulate	Plag (An_{30})	Pig VB-16 (*mg*-no. 0·62)	Cpx (*mg*-no. 0·67)	Ilm (Hem_0)	Mgt ($Uvsp_{31}$)	Apa
SiO_2	57·02	65·71	39·93	61·00	51·66	51·06	0·40	1·22	0·00
TiO_2	1·92	0·99	4·32	0·00	0·78	0·51	52·79	11·05	0·00
Al_2O_3	14·16	13·31	12·33	24·70	1·27	2·36	0·10	2·13	0·00
FeO_t	11·98	7·54	21·91	0·00	20·30	11·51	45·05	79·50	0·00
MgO	1·71	0·65	4·75	0·00	18·20	13·04	1·31	0·91	0·00
CaO	4·71	2·56	9·29	6·10	7·67	21·00	0·08	0·16	56·79
Na_2O	3·35	3·07	3·47	7·20	0·11	0·53	0·00	0·00	0·00
K_2O	3·64	5·04	0·47	1·00	0·00	0·00	0·00	0·00	0·00
P_2O_5	1·05	0·51	2·59	0·00	0·00	0·00	0·00	0·00	43·21
$\Sigma r^2 = 0{\cdot}057$									

*For stage 2, the starting composition corresponds to the average of several evolved jotunites including 75202F and 7355 whereas the mangerite is the average of the Kungland facies of the Lomland dike (Duchesne *et al.*, 1985).
†For stage 3, the starting and final compositions are samples 7828 and 7832 of the Tellnes dike, respectively (Wilmart, 1988; Wilmart *et al.*, 1989).

'magma' instead of 'liquid'. The composition of this parent magma is given in Table 6 (evolved jotunite). Calculation of the virtual olivine composition, using the Ford *et al.* (1983) relationship, in equilibrium with that liquid gives Fo_{56} at 5 kbar (1094°C). This olivine constrains the *mg*-number of the pyroxenes in equilibrium with that liquid and permits selection of the other minerals (plag, ilm and magnetite) in the series of BKSK cumulate

assemblages. Given these compositions, it is possible to calculate by least-squares fitting the proportions of the minerals in the cumulate which subtracted from an evolved jotunitic liquid close to VB give a mangeritic composition close to that of the Lomland dike (Klungland facies) which is also close to that of sample 78211 (2·7% MgO). The fitting is excellent (sum of the squared residues <0·1). The composition of the assemblage is given in Table 6, as well as the whole-rock composition of the calculated cumulate and the mangeritic composition. It is worth noting that this latter composition is close to the melt phase obtained in the VB-16 run in which the cumulate is also very rich in oxide [53% plag + 7·5% pig + 7·5% aug + 25% uvsp + 7·5% phosph: uvsp is the sole oxide as the experiment was conducted at NNO and the proportion of pyroxenes is less than in the calculated cumulate because the VB-16 liquid is higher in SiO_2 (56·69%) than the calculated mangerite (51·60%)]. On the other hand, the noritic cumulate deduced from trace element modeling of the second stage (noritic) of BKSK (Duchesne, 1978) as well as the noritic cumulate calculated for the Tellnes dike (Wilmart *et al.*, 1989) bracket the assemblage calculated here.

In a study of the Tellnes dike, Wilmart *et al.* (1989) have modeled the formation of a charnockite from an evolved jotunite (similar to VB). The presence of a quartz mangerite (7838) among the series of fine-grained samples confirms the general nature of this differentiation process. Stage 3 of our modeling, which employs samples 7828 (mangerite) and 7832 (quartz mangerite) from the Tellnes dike (Wilmart *et al.*, 1989) as the starting and final compositions, respectively, is now a refinement of their calculations. The results show that an oxide–gabbro cumulate (C3; Table 6) can account for fractionation from a mangerite to a quartz mangerite. The C3 plagioclase contains 1% K_2O, in agreement with the VB-16 plagioclase (0·80% K_2O). Petrographic and experimental data indicate that olivine is not stable in the evolved liquids of the differentiation trend, which justifies the presence of pigeonite instead of olivine (Wilmart *et al.*, 1989) in our cumulate. Mass balance calculations thus indicate that differentiation and silica enrichment along the jotunitic trend can be explained by extraction of magnetite–ilmenite-rich cumulates (C2 and C3) whose bulk SiO_2 values are lower than that of the evolved jotunite and mangerite, as already pointed out by Hunter & Sparks (1987) for the Skaergaard intrusion. This conclusion is further supported by several other lines of evidence. As already mentioned, the mangeritic liquid of run VB-16 is in equilibrium with an assemblage containing 25% uvsp. Moreover, the BKSK evolved cumulates are characterized by thick layers of ultramafic rock containing up to 50% of Fe–Ti oxides, interleaved with norites or mangerites (Duchesne *et al.*, 1987). Finally, the calculated cumulates are close to sample MEL, and the occurrence of FTP rocks such as MEL indicates that it is possible to accumulate large amounts of Fe–Ti oxides from these magmas.

Constraints from trace elements

We have also modeled the abundances of various trace elements (REE, Sr, U, Th, Zr, Hf, Ta, Rb, Ba, Co, Ni, Cr, Sc) in three stages using the same proportions of minerals that proved successful for the major elements. Partition coefficients are listed in Tables 7 and 8, and are taken from the literature, except where noted. Apatite and plagioclase are likely to be the most important phases because apatite has the highest D_{REE} values of the calculated minerals (Watson & Green, 1981), whereas plagioclase is the most abundant phase in the model cumulates, and apatite and plagioclase fractionate Eu and Sr relative to the REE in opposite directions. We have attempted to account for compositional variations in partition coefficients and to fill in gaps in the experimental data base with various approximations. For example, D_{Eu} (plag) has been calculated using Drake's equation (Drake, 1975) taking $D_{Eu2+} = D_{Sr} = 1{\cdot}4$ (Watson & Green, 1981) and determining D_{Eu3+} by extrapolating the other trivalent REE. The set of D_{REE} (plag) (Table 7) has been estimated by normalizing trace element concentrations measured in plagioclase separates (An_{50}) from the anorthositic cumulates of the Hidra leuconoritic body (Demaiffe & Hertogen, 1981) to concentrations of the same elements in Hidra chilled margin samples (Duchesne *et al.*, 1974; Demaiffe & Hertogen, 1981). In the case of apatite in stage 2, for example, the D_{REE} values have been calculated by normalizing the REE concentrations of apatite separated from sample MEL to the REE concentrations of bulk sample 8951, which is close to a liquid composition. For stage 3, the data of Fujimaki (1986) have been adopted.

Results of the model calculations using sample 80123a [TJ: Duchesne & Hertogen (1988); Vander Auwera & Longhi (1994)] as the starting composition are shown in Figs 9 and 10. The REE (Fig. 9a) show a strong increase during stage 1, then decrease from stage 2 to stage 3 as apatite crystallizes. A slight negative Eu anomaly appears in stage 1 and then disappears in stage 2 as a result of the appearance of apatite in the cumulate. Finally, fractionation of apatite with high D values in stage 3 induces the appearance of a positive Eu anomaly. The calculated REE contents closely, but not exactly, match the patterns observed in the jotunitic suite (Fig. 6). Small positive Eu anomalies in some evolved jotunites and lack of any Eu anomaly in others probably reflect minor accumulations of plagioclase in the evolved jotunites inferred from phase equilibria considerations. For the other trace elements, results are shown in Fig. 9b and

Table 7: REE partition coefficients selected for the modeling

	plag (1)	apa,2 (2)	apa,3 (3)	opx (4)	cpx (5)	ilm (6)	mgt (1)
La	0·13	12·0	14·5	0·0019	0·04	0·0023	0·006
Ce	0·11	15·0	21·1	0·0035	0·075	0·0019	0·006
Pr	0·1	17·0	26·9	0·0059	0·113	0·0016	0·006
Nd	0·09	19·0	32·8	0·013	0·15	0·0012	0·006
Sm	0·06	20·0	46·0	0·063	0·22	0·0023	0·006
Eu	0·46	13·0	25·5	0·059	0·2	0·0009	0·006
Gd	0·052	20·0	43·9	0·069	0·25	0·006	0·006
Tb	0·05	19·0	39·4	0·11	0·258	0·0095	0·006
Dy	0·048	18·0	34·8	0·15	0·267	0·013	0·006
Ho	0·046	16·8	28·8	0·2	0·275	0·022	0·006
Er	0·044	15·5	22·7	0·24	0·283	0·031	0·006
Tm	0·042	14·2	19·1	0·315	0·292	0·044	0·006
Yb	0·04	13·0	15·4	0·39	0·3	0·057	0·008
Lu	0·038	10·0	13·8	0·47	0·3	0·07	0·008

1, Demaiffe & Hertogen (1981); 2, see text for explanation; 3, Fujimaki (1986); 4, Dunn & Sen (1994); 5, McKay (1989) for 40% Wo; 6, Nakamura *et al.* (1986); 2 and 3 correspond to the cumulates c2 and c3 of Table 6. Values of *D* not given in the literature were extrapolated.

Table 8: Trace elements partition coefficients selected for the modeling

	plag1	plag2	plag3	opx	ilm	apa2	apa3	cpx	mgt
Sr	1·9 (1)	2·3 (1)	3·9 (1)	0·0034 (2)		1·4 (3)	2·2 (3)	0·09 (5)	
U	0·34 (2)	0·34 (2)	0·34 (2)	0·0002 (8)		25 (12)	25 (12)	0·0009 (13)	
Th	0·04 (6)	0·04 (6)	0·04 (6)	0·0001 (8)	*0·09*	*23*	*19*	0·0015 (13)	0·025 (19)
Zr				0·021 (2)	0·33 (10)			0·25 (14)	0·12 (19)
Hf	0·01 (7)	0·01 (7)	0·01 (7)	0·004 (8)	0·419 (10)			0·29 (15)	0·97 (19)
Ta	0·018 (6)	0·018 (6)	0·018 (6)	0·004 (21)	*3·7*			*0·03*	*0·04*
Rb	0·1 (6)	0·1 (6)	0·1 (6)	0·025 (4)					
Ba	0·38 (2 & 22)	0·38 (2 & 22)	0·38 (2 & 22)	0·00015 (8)				0·0023 (16)	
Co	0·05 (6)	0·05 (6)	0·05 (6)	0·7 (8)	*9*			1·2 (4)	5 (20)
Ni				9·5 (8)	*17*			2 (17)	44 (19)
Cr	0·03 (7)	0·03 (7)	0·03 (7)	1 (8)	16 (11)			2·7 (18)	350 (11)
Sc	0·015 (7)	0·015 (7)	0·015 (7)	2 (9)	2 (9)			4 (9)	2 (9)

(1) Duchesne (1978) and Vander Auwera *et al.* (1993); (2) Dunn & Sen (1994); (3) Watson & Green (1981); (4) Henderson (1982); (5) Ray *et al.* (1983); (6) calculated from Demaiffe & Hertogen (1981) and Duchesne *et al.* (1974); (7) Phinney & Morrison (1990); (8) Kennedy *et al.* (1993); (9) Duchesne *et al.* (1985); (10) McKay *et al.* (1986); (11) Jensen *et al.* (1993); (12) J. C. Duchesne, personal communication (1996); (13) Beattie (1993); (14) Johnson & Kinzler (1989); (15) Hart & Dunn (1993); (16) average of values given by Hart & Dunn (1933), Beattie (1993) and Hauri *et al.* (1994); (17) Steele & Lindstrom (1981); (18) average of values given by Hart & Dunn (1993) and Hauri *et al.* (1994); (19) Nielsen *et al.* (1994); (20) Horn *et al.* (1994); (21) Forsythe *et al.* (1994); (22) Duchesne & Demaiffe (1978). 1, 2 and 3 are for the three cumulates c1–c3 of Table 6. When the *D* value is not specified in a mineral, it is assumed equal to zero. Partition coefficients in italics have been calculated.

compared with the observed compositions of the different types of rocks in Table 9. Sr, U, Th, Co, Ni and Cr decrease with fractionation; Zr, Hf, Rb and Ba increase; Ta slightly increases; and, finally, Sc displays a slight increase in the first stage and then decreases in the subsequent stages as magnetite crystallizes. The uniformly incompatible nature of Zr and Hf suggests that zircon is not a liquidus phase in the jotunitic suite. These results

Table 9: Comparison between observed and calculated trace element content

	Primitive jotunites		Evolved jotunites		Mangerites		Quartz mangerites	
	80123a	Observed range	Calculated	Observed range	Calculated	Observed range	Calculated	Observed range
Sr	530	382–784	400	412–465	377	272–310	257	128–211
U	0·10	0·1–1·3	0·17	0·32	0·09	0·1–18	0·08	0·1–0·2
Th	0·50	0·5–3·8	0·97	0·51–1·19	0·63	0·59–0·67	0·63	0·66–0·87
Zr	262·00	155–292	510·96	89–558	821·85	717–952	1193·36	1251–1387
Hf	6·50	4·5–8·2	12·56	5·4–11	19·10	17·3–22·1	25·71	28·5–32·5
Ta	1·31	0·8–1·31	2·01	1–2·2	2·78	1·3–1·9	3·95	0·94–1·62
Rb	17·00	5·8–44	32·21	9·7–13·4	52·38	34	76·63	48–71
Ba	469·00	469–801	771·87	1065–1602	1182·61	1533–1801	1643·05	1842–1979
Co	49·00	30–72·9	47·36	34·7–56·9	33·76	17–20·2	26·96	7·2–11·5
Ni	60·00	53–60	12·88	6·6–16·1	0·27	0–1·4	0·00	
Cr	28·00	28–50	16·28	22–66	0·00	4–34	0·00	1–21
Sc	13·80	13·8–25·9	19·10	8·15–28·1	17·69	19–21·1	16·20	16–17·7

For each type of rock, the composition calculated using the three-stage major element model (see text for explanation) is compared with the range observed in the fine-grained samples. In the case of the primitive jotunites, these samples are 80123a, 7234, 91141; 7020 (Duchesne *et al.*, 1974); 200/22, 259/11 (Demaiffe & Hertogen, 1981); B90, B93, B95 (Wilson *et al.*, 1996). For the evolved jotunites, the samples are 75202F, 7355, 89115, 8925, 8926 as well as 7252 (Wilmart *et al.*, 1989). For the mangerites, the samples are 7838 and 7832 (Wilmart *et al.* 1989).

are similar to those obtained for the Tellnes dike (Wilmart, 1988; Wilmart *et al.*, 1989). For most elements the agreement between observed and calculated values is very good, which supports the major element modelling proposed above. It should be noted especially that the Sr concentration decreases with crystallization, whereas the LREE show a small overall increase; hence the development of a pronounced Sr depletion relative to the LREE in the most evolved rocks—a clear sign of plagioclase fractionation. Continuous enrichment of Hf and Zr smooths out the depletions of Hf and Zr relative to the middle REE (MREE) in the transition from evolved jotunite to quartz mangerite as observed in the rocks (Fig. 7). For U and Th, our calculated values increase in stage 1 and then slowly decrease in stages 2 and 3, as observed in the rocks, reflecting the crystallization of apatite in stages 2 and 3, with high partition coefficients for these elements (Duchesne & Wilmart, 1997). Also, the calculated Rb concentration increases as expected with differentiation, but, starting with 17 ppm in 80123a, the concentrations after stages 1 and 2 are higher than those measured in the evolved jotunites and the mangerites. When a starting composition lower in Rb is chosen, as, for example, 5·80 ppm in primitive jotunite 91141, the calculated values in stages 2 (17·87 ppm) and 3 (26·17 ppm) are lower than the observed ranges. The highly variable Rb contents of the primitive jotunites (Duchesne *et al.*, 1989) probably reflect different degrees of contamination in the various batches of the parental jotunite magma. Although some additional contamination during fractionation of the Varberg and Lomland dikes cannot be excluded, Rb–Sr isotopic data prohibit any significant contamination of the Tellnes dike during fractionation (Wilmart *et al.*, 1989). The same conclusion can also be drawn regarding the K_2O evolution. Small variations in the K_2O content of the parental magma batches, noted by Duchesne *et al.* (1989), are amplified by fractionation of a low-K cumulate. Contamination of the dikes is curious because most of the outcrop of the jotunitic dikes lies within anorthositic rocks which are very low in K and Rb. The unsuitability of the anorthosite as a source of contamination for the dikes suggests that the dikes intruded the anorthosites already contaminated.

DISCUSSION

Results presented here indicate that quartz mangerites occurring in the vicinity of anorthositic complexes can be produced by extensive fractionation of primitive jotunites. Their compositions will be dependent upon the composition of the parental jotunite, but some generalizations are possible: such quartz mangerites will be characterized by REE concentrations in the range of jotunites with a weak Eu anomaly that is more positive (or less negative)

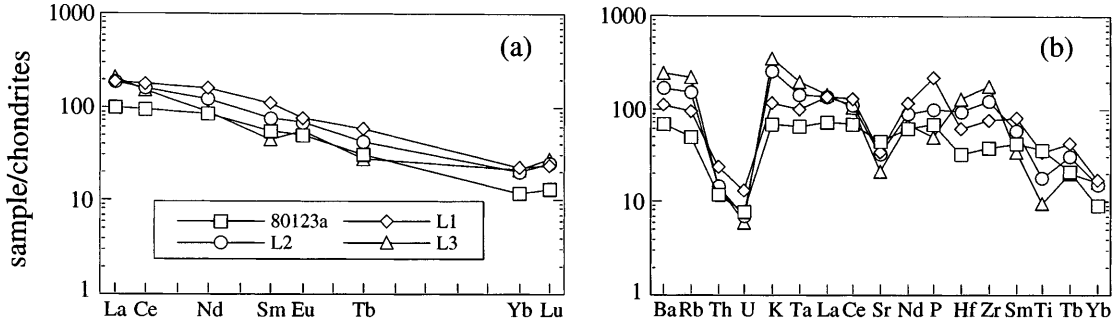

Fig. 9. Calculated REE (a) and trace elements (b) content of the evolved jotunite (L1), the mangerite (L2) and the quartz mangerite (L3) using sample 80123a as a starting composition and the three cumulates deduced from the major element modeling (in Table 6). Partition coefficients used in the model are given in Tables 7 and 8.

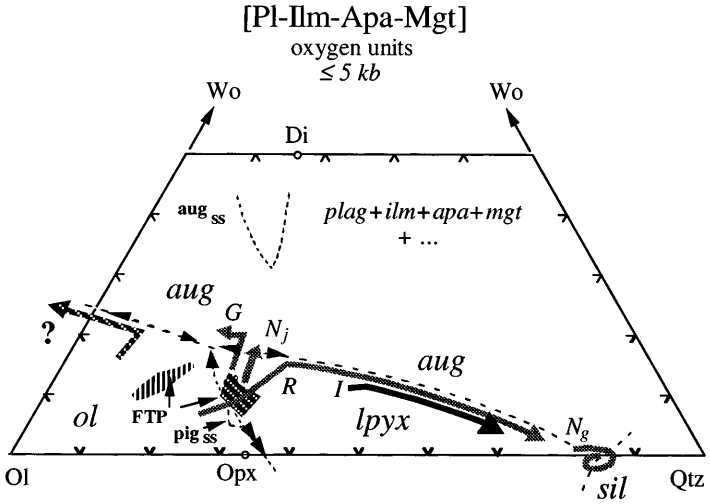

Fig. 10. Schematic representation of liquidus equilibria of ilmenite–apatite–magnetite–plagioclase saturated liquids projected onto the olivine–wollastonite–quartz plane. Arrows show direction of decreasing temperature; single arrows indicate cotectics; double arrows indicate reaction curves. Shaded paths indicate lines of descent consistent with mineral assemblages as explained in text. *G*, Laramie and Marcy trends; *Nj*, Nain jotunite (ferrodiorite) trend; *Ng*, Nain granitoids; *R*, Rogaland trend (see text); *I*, hypothetical trend of crustal melt with intermediate composition.

than its parent; and on multi-element plots there will be locally strong depletions of U, Th, Sr, and Ti with smaller to no relative depletions of Hf and Zr. Complementary to the quartz mangerite will be a series of cumulates rich in oxides and apatite which will form melanocratic rocks. Recently, Owens *et al.* (1993) described a broadly similar scenario for derivation of quartz mangerite from jotunite in the Grenville Province of Quebec. These observations differ in detail from those of Mitchell *et al.* (1996) and Emslie *et al.* (1994). Mitchell *et al.* (1996) described monzodiorite (~jotunite) evolving to monzonite (mangerite) and then monzosyenite instead of quartz monzonite (~quartz mangerite) along with the formation of complementary oxide–apatite-rich rocks in the Laramie Complex of Wyoming. Emslie *et al.* (1994) observed an absence of evolved compositions in the range of 52–62 wt % SiO_2, but a continuum in SiO_2 from 62 (quartz mangerite) to 74% (charnockite) in the Nain Complex of Labrador. Not surprisingly, Emslie *et al.* (1994) ascribed their high-Si compositions to partial melting of the lower crust, not fractionation. The Nain high-Si compositions have much in common with the Rogaland quartz mangerites in terms of mineralogy and trace element abundance patterns; however, the Nain granitoids show small negative Eu anomalies and more pronounced relative depletions of Sr and P, which might reflect more extensive fractionation of plagioclase and apatite, but might also reflect partial melting of a mafic crustal source. Also, the Rogaland quartz mangerites are found only within fractionated dikes or as the upper portion of a much larger jotunitic

intrusion such as BKSK (Duchesne & Wilmart, 1997), whereas some of the Nain granitoids comprise entire discrete intrusions or substantial fractions of others. Although the difference in field relations between Rogaland and Nain may be due in part to the level of exposure, we cannot exclude the possibility of deriving some quartz mangerites by partial melting of the lower crust. Indeed, as discussed below, there is a wide range of pressure and composition for which fractionation of a jotunitic magma cannot yield quartz mangerite.

Our conclusions on the liquid line of descent of jotunites, as well as those of Owens *et al.* (1993) and Mitchell *et al.* (1996), contradict those presented by McLelland *et al.* (1994), who modeled the compositions of P–Ti–Fe-rich mafic dikes and sheets from the contact zone of the Marcy massif in the Adirondack mountains. In variation diagrams, the trends defined by these rocks show extreme enrichments in FeO_t (up to 25%), TiO_2 (up to 7·6%), P_2O_5 (3·6%) correlated with extreme depletion in silica (down to 36% SiO_2). McLelland *et al.* (1994) admitted that these rocks are likely to represent crystal-laden liquids but nevertheless contended that the liquid line of descent followed at least in part a trend of decreasing Si and increasing P, Ti, and Fe. However, comparison with the data from this study indicates that the highest Fe, Ti, P and lowest Si concentrations are similar to those of Rogaland sample MEL, which is demonstrably a partial cumulate of a multiphase liquidus assemblage (pyroxene, apatite, ilmenite, magnetite); furthermore, experiments show that FeO_t, TiO_2, and P_2O_5 decrease as oxides and apatite crystallize from this composition. In projections such as Fig. 4a and b, the FTP-rich model magmas M6–M9 from McLelland *et al.* (1994) (Table 1) define a trend (not shown) pointing away from the 5 kbar pseudo-eutectic toward the Ol component; whereas model magmas M4–M6 plot close to the pseudo-eutectic. As explained above, the highest apparent contents of the Ol component may be in part a mixture of pyroxene and magnetite. The presence of pyroxene + oxide + apatite + plagioclase in M8 followed by the initial appearance of olivine in M9 is also consistent with a eutectic-like pseudo-invariant point. Thus the Marcy FTP enrichment is due primarily to accumulation from a multisaturated jotunitic liquid.

Interestingly, McLelland *et al.* (1994) pointed out the existence of a 'coeval, but not comagmatic' suite of rocks including mangerites and charnockites, which suggests a second jotunitic magma series characterized by silica enrichment similar to Rogaland (e.g. De Waard & Romey, 1968). The various differentiation paths of these and other jotunitic suites are illustrated in Fig. 10 by schematic versions of Fig. 4a in which magnetite is included as a projection component. The overall topology of Fig. 10 is the same as in Fig. 4a, but points project differently (higher Qtz component) because some of the Fe has been removed from the Ol component to form an Fe_3O_4 (Mgt) component. Liquid lines of descent are represented by shaded lines and FTP trends by patterned areas. Because different suites probably crystallized at different pressures the topology of the entire diagram may not be appropriate to a single pressure or composition (with decreasing pressure or increasing *mg*-number the olivine pseudo-eutectic becomes peritectic and the pyroxene–plagioclase thermal divide disappears). However, the diagram was constructed such that the local liquidus topologies would be appropriate. The diagram shows that the plagioclase + low-Ca pyroxene + augite thermal maximum is stable on the aug + lpyx liquidus boundary and that the Wo-rich portion of the ol + lpyx curve is even, whereas the low-Wo portion is odd and truncates the thermal ridge that crosses the lpyx liquidus field. This configuration allows olivine to react out of magmas along the *R* curve and be replaced by pigeonite (lpyx); and it also allows the fractionating magma to eventually reach silica saturation—Rogaland, some of the Grenville intrusions (Owens *et al.*, 1993) and parts of the Adirondacks (De Waard & Romey, 1968) are examples. The *G* curve represents magmas in which olivine crystallizes after pigeonite at the pseudo-eutectic, such as in the Greaser Intrusion in the Laramie Complex (Mitchell *et al.*, 1996) and the Marcy trend of McLelland *et al.* (1994). The N_j curve [Nain—Emslie *et al.* (1994); Maloin Ranch pluton—Kolker & Lindsley (1989)] is an example of a trend in which the liquid lies in the pyroxene + plagioclase thermal divide, so neither olivine nor quartz crystallizes, even after extensive fractionation. As a result, jotunitic (ferrodioritic, monzonoritic) rocks grade into two-pyroxene mangerites, and subsequently into syenites. Such rocks will show a modest increase in SiO_2 concentration because the high-Si felsic components increase at the expense of the low-Si mafic components in the residual liquids (e.g. Longhi, 1991). Because the decrease in the Qtz component is so small along the *G* trend, SiO_2 will also increase weakly in the residual liquid as it progressively forms olivine-free jotunites (ferrodiorites), olivine-bearing mangerites, and ol syenites. Thus FTP cumulates apparently have developed from liquids that underwent pronounced SiO_2 enrichment (*R*) as well as from residual liquids in which SiO_2 increased only modestly (N_j, *G*). Finally, the curve labeled with the question mark is an example of a line of descent along which SiO_2 concentration and Qtz content decrease, and FeO_t, TiO_2 and P_2O_5 increase, even though ilmenite and apatite are crystallizing. Such behavior is possible because the solubilities of TiO_2 and P_2O_5 increase with decreasing SiO_2 (e.g. Harrison & Watson, 1984). Rocks formed from such magmas would contain olivine, plagioclase, and highly aluminous augite, in addition to apatite and oxides, but no low-Ca pyroxene. We are not aware of any

examples of such a rock series in Proterozoic anorthosite complexes.

It follows that lpyx-bearing granitoids cannot be consanguinous with coeval jotunitic rocks, if the parent magma of the jotunites evolved either on the low-Qtz side of the pyroxene–plagioclase thermal divide (e.g. *G*) or in the divide itself (e.g. N_j). Charnockitic granitoids could only have been derived from parent magmas that project to the high-Qtz side of the thermal divide; there are three possible options: (1) the granitoid magmas may have fractionated from a jotunitic liquid with low-Wo content like TJ that was able to breach the trace of the thermal divide before low-Ca pyroxene precipitated (*R*); (2) they may have fractionated from crustal melts with intermediate composition (*I*); (3) the granitoids may have crystallized directly from high-SiO_2 crustal melts (N_g), as suggested by Emslie *et al.* (1994). In the first case, continuous variation in SiO_2 concentration is expected. In the second case, a gap in SiO_2 is problematical; however, a bimodal volume distribution vs SiO_2 is likely even if SiO_2 variation is apparently continuous. In the third case, a gap in SiO_2 concentration is inevitable.

CONCLUSIONS

The Rogaland jotunitic trend presented above (Fig. 2) is the latter part of a multi-stage process of polybaric fractional crystallization, crystal accumulation, and probably flow differentiation within dikes. The high MgO–FeO_t–TiO_2–P_2O_5 rocks are accumulations of a dense oxide–apatite–pigeonite assemblage into coexisting jotunitic to mangeritic liquids. The accumulation is probably the result of flow differentiation within the dike system causing separation of a crystal-rich suspension into high- and low-density components, liquid $\pm$ plagioclase being the low-density component. Indeed, the dike chill margins appear to be mixtures of multi-saturated liquid and 15–30% plagioclase. Evidence of K and Rb increasing faster than can be accounted for by fractional crystallization suggests contamination of the suspension before its intrusion into the anorthositic terrane. Estimated CaO concentrations of the bulk compositions of inverted pigeonites are intermediate to those produced at 1 bar and those at 5 kbar, suggesting crystallization of the Varberg dike, at least, in this pressure range. The earlier part of the process was fractional crystallization of a primitive jotunitic magma that is similar to the parental liquid of the Bjerkreim–Sokndal layered intrusion. Major and trace element modeling are consistent with extraction of an ilmenite–norite component from the primitive jotunite to form an evolved jotunite similar to the Varberg chill margin. Liquids generated in melting experiments (Vander Auwera & Longhi, 1994) on a primitive jotunite (TJ) at 5–7 kbar are saturated not only with the requisite ilmenite–norite assemblage, but also intersect the jotunite major element trend closest to the Varberg chill margin composition. Trace element modeling also is consistent with such a scheme. This early stage of fractionation probably took place several kilometers below the intrusion level of dikes in a chamber evolving similarly to BKSK and provides the link between primitive and evolved jotunites.

Other researchers have argued that the jotunitic (ferrodioritic) suite was derived by fractionating liquids residual to the anorthosites themselves (e.g. Owens *et al.*, 1993; Mitchell *et al.*, 1996). Although we have presented evidence from Rogaland that seemingly contradicts these arguments in detail, we agree in the larger sense because we believe that primitive jotunites may be parental not only to mafic bodies such as BKSK, but also to a substantial portion of the Rogaland anorthosites (Duchesne, 1978; Longhi & Vander Auwera, 1992)—the amount of suspended plagioclase determines whether the intrusion is anorthositic or mafic, but the liquid is similar and so is its line of descent. Thus the jotunitic dikes may just as well have been spawned by fractionation within a deep-seated anorthositic intrusion as in a layered, mafic body similar to BKSK. Furthermore, although there is widespread belief that a mantle-derived high-Al basalt is parental to the massif anorthosites (Morse, 1982; Emslie *et al.*, 1994; Mitchell *et al.*, 1996), there is evidence of a continuum in composition between such high-Al basalts and primitive jotunites, which have higher concentrations of Ti, P, and K but are otherwise similar (Longhi & Vander Auwera, 1992). And, most importantly, both high-Al basaltic and primitive jotunitic compositions, which are suitable as parental magmas of anorthosites, lie in thermal divides (maxima) at lower crustal pressures, which effectively precludes their having been derived by fractional crystallization, with or without crustal assimilation, of more primitive mantle derived melts (Longhi & Vander Auwera, 1992).

Further crystallization and flow of the evolved jotunitic magma within the dikes produced a series of mangeritic, quartz mangeritic, and charnockitic rocks displaying a continuous increase in SiO_2 concentration. There are also low-SiO_2 facies of the dikes enriched in FeO_t, TiO_2, and P_2O_5 (FTP rocks), which are partial cumulates of pigeonite, oxides, and apatite complementary to the SiO_2 enrichment trend. Trace element modeling of this fractionation scheme closely reproduces the observed rock compositions, in particular the lack of a significant Eu anomaly despite extensive plagioclase fractionation. Whether jotunitic magmas fractionate continuously to quartz mangerite and charnockite or to mangerite and syenite is determined by their disposition relative to the pyroxene–plagioclase thermal divide, which becomes stable at ~3–4 kbar in these compositions. Jotunitic magmas that crystallize either in the thermal divide or

on the low-Qtz side of the divide will not yield high-SiO_2, quartz-bearing derivatives; consequently, coeval granitoids are either direct crustal melts or derived from crustal melts with intermediate composition. If low-pressure and/or low Wo content permit a jotunitic magma to breach the pyroxene–plagioclase thermal divide, then continued fractionation will yield consanguinous granitoids as in Rogaland.

ACKNOWLEDGEMENTS

We would like to thank J. L. Joron for analysing some samples, as well as G. Bologne and G. Delhaze for help with the chemical analyses and sample preparation. The microprobe analyses were performed under the supervision of G. Wauthier. Financial support to J.V.A. and J.C.D. was provided by the Belgian Fund for Joint Basic Research, and to J.L. by NASA Grants NAG-9-329 and NAGW 3407. This work was also part of the International Geological Correlation Program, Project 290. This paper is Lamont–Doherty Earth Observatory Contribution 5741.

REFERENCES

Andersen, D. J. & Lindsley, D. H. (1988). Internally consistent models for Fe–Mg–Mn–Ti oxides: Fe–Ti oxides. *American Mineralogist* **73,** 714–726.

Ashwal, L. D. (1982). Mineralogy of mafic and Fe–Ti oxide-rich differentiates of the Marcy anorthosite massif, Adirondacks, NY. *American Mineralogist* **67,** 14–27.

Ashwal, L. D. (1993). *Anorthosites*. Berlin: Springer-Verlag.

Beattie, P. (1993). The generation of uranium series disequilibria by partial melting of spinel peridotite: constraints from partitioning studies. *Earth and Planetary Science Letters* **117,** 379–391.

Bolle, O. (1996). The Apophysis of the Bjerkreim–Sokndal layered intrusion (southwestern Norway). In: Demaiffe, D. (ed.) *Petrology and Geochemistry of Magmatic Suites of Rocks in the Continental and Oceanic Crusts (J. Michot volume)*. Bruxelles: MRAC & ULB, pp. 129–144.

Bologne, G. & Duchesne, J. C. (1991). Analyse des roches silicatées par spectrométrie de fluorescence X: précision et exactitude. *Belgian Geological Survey Professional Paper* **249,** 11 pp.

Demaiffe, D. & Hertogen, J. (1981). Rare earth geochemistry and strontium isotopic composition of a massif-type anorthositic–charnockitic body: the Hidra massif (Rogaland, SW Norway). *Geochimica et Cosmochimica Acta* **45,** 1545–1561.

Demaiffe, D., Weis, D., Michot, J. & Duchesne, J. C. (1986). Isotopic constraints on the genesis of the Rogaland anorthositic suite (southwest Norway). *Chemical Geology* **57,** 167–179.

De Waard, D. & Romey, W. D. (1968). Petrogenetic relationships in the anorthosite–charnockite series of Snowy Mountain Dome, south–central Adirondacks. In: Isachsen, Y. W. (ed.) *Origin of Anorthosite and Related Rocks. New York State Museum and Science Service, Memoir* **18,** 307–315.

Drake, M. J. (1975). The oxidation state of europium as an indicator of oxygen fugacity. *Geochimica et Cosmochimica Acta* **39,** 55–64.

Duchesne, J. C. (1972*a*). Iron–titanium oxide minerals in the Bjerkreim–Sogndal Massif, south-western Norway. *Journal of Petrology* **13,** 57–81.

Duchesne, J. C. (1972*b*) Pyroxènes et olivines dans le massif de Bjerkreim–Sogndal (Norvège méridionale). Contribution à l'étude de la série anorthosite–mangérite. *24th International Geological Congress, Montreal Section 2,* **2**, pp. 320–328.

Duchesne, J. C. (1978). Quantitative modeling of Sr, Ca, Rb and K in the Bjerkreim–Sogndal lopolith (SW Norway). *Contributions to Mineralogy and Petrology* **66,** 175–184.

Duchesne, J. C. (1990). Origin and evolution of monzonorites related to anorthosites. *Schweizerische Mineralogische und Petrographische Mitteilungen* **70,** 189–198.

Duchesne, J. C. (1998). Fe–Ti deposits in Rogaland anorthosites (south Norway): geochemical characteristics and problems of interpretation. In: Rickard, D. (ed.) *Agricola Volume*. New York: John Wiley.

Duchesne, J. C. & Demaiffe, D. (1978). Trace elements and anorthosite genesis. *Earth and Planetary Science Letters* **38,** 249–272.

Duchesne, J. C. & Hertogen, J. (1988). Le magma parental du lopolithe de Bjerkreim–Sokndal (Norvège méridionale). *Comptes Rendus Hebdomadaires des Séances de l'Académie des Sciences* **306**(2), 45–48.

Duchesne, J. C. & Wilmart, E. (1997). Igneous charnockites and related rocks from the Bjerkreim–Sokndal layered intrusion (Southwest Norway): a jotunite (hypersthene monzodiorite)-derived A-type granitoid suite. *Journal of Petrology* **38,** 337–369.

Duchesne, J. C., Roelandts, I., Demaiffe, D., Hertogen, J., Gijbels, R. & de Winter, J. (1974). Rare-earth data on monzonoritic rocks related to anorthosites and their bearing on the nature of the parental magma of the anorthositic series. *Earth and Planetary Science Letters* **24,** 325–335.

Duchesne, J. C., Roelandts, I., Demaiffe, D. & Weis, D. (1985). Petrogenesis of monzonoritic dykes in the Egersund–Ogna anorthosite (Rogaland, SW Norway): trace elements and isotopic (Sr, Pb) constraints. *Contributions to Mineralogy and Petrology* **90,** 214–225.

Duchesne, J. C., Denoiseux, B. & Hertogen, J. (1987). The norite–mangerite relationships in the Bjerkreim–Sokndal layered lopolith (southwest Norway). *Lithos* **20,** 1–17.

Duchesne, J. C., Wilmart, E., Demaiffe, D. & Hertogen, J. (1989). Monzonorites from Rogaland (Southwest Norway): a series of rocks coeval but not comagmatic with massif-type anorthosites. *Precambrian Research* **45,** 111–128.

Dunn, T. & Sen, C. (1994). Mineral/matrix partition coefficients for orthopyroxene, plagioclase, and olivine in basaltic to andesitic systems: a combined analytical and experimental study. *Geochimica et Cosmochimica Acta* **58,** 717–733.

Emslie, R. F. (1985). Proterozoic anorthosite massifs. In: Tobi, A. C. & Touret, J. L. R. (eds) *The Deep Proterozoic Crust in the North Atlantic Provinces. NATO Advanced Study Institute C158*. Dordrecht: D. Reidel, pp. 39–60.

Emslie, R. F., Hamilton, M. A. & Thériault, R. J. (1994). Petrogenesis of a Mid-Proterozoic Anorthosite–Mangerite–Charnockite–Granite (AMCG) complex: isotopic and chemical evidence from the Nain Plutonic Suite. *Journal of Geology* **102,** 539–558.

Ford, C. E., Russell, D. G., Craven, J. A. & Fisk, M. R. (1983). Olivine–liquid equilibria: *T*, *P* and composition dependence of the crystal/liquid cation partition coefficients for Mg, Fe, Ca and Mn. *Journal of Petrology* **24**(3), 256–265.

Forsythe, L. M., Nielsen, R. L. & Fisk, M. R. (1994). High-field-strength element partitioning between pyroxene and basaltic to dacitic magmas. *Chemical Geology* **117,** 107–125.

Fram, M. & Longhi, J. (1992). Phase equilibria of dikes associated with Proterozoic anorthosite complexes. *American Mineralogist* **77,** 605–616.

Fujimaki, H. (1986). Partition coefficients of Hf, Zr and REE between zircon, apatite and liquid. *Contributions to Mineralogy and Petrology* **94,** 42–45.

Ghiorso, M. S. & Sack, R. O. (1995). Chemical mass transfer in magmatic processes. IV. A revised and internally consistent thermodynamic model for the interpolation and extrapolation of liquid–solid equilibria in magmatic systems at elevated temperatures and pressures. *Contributions to Mineralogy and Petrology* **119,** 197–212.

Harrison, T. M. & Watson, E. B. (1984). The behavior of apatite during crustal anatexis: equilibrium and kinetic considerations. *Geochimica et Cosmochimica Acta* **48,** 1467–1477.

Hart, S. R. & Dunn, T. (1993). Experimental cpx/melt partitioning of 24 trace elements. *Contributions to Mineralogy and Petrology* **113,** 1–8.

Hauri, E. H., Wagner, T. P. & Grove, T. L. (1994). Experimental and natural partitioning of Th, U, Pb and other trace elements between garnet, clinopyroxene and basaltic melts. *Chemical Geology* **117,** 149–166.

Henderson, P. (1982). *Inorganic Geochemistry*. Oxford: Pergamon Press.

Hoover, J. (1989). The chilled marginal gabbro and other contact rocks of the Skaergaard intrusion. *Journal of Petrology* **30**(2), 441–476.

Horn, I., Foley, S. F., Jackson, S. E. & Jenner, G. A. (1994). Experimentally determined partitioning of high field strength- and selected transition elements between spinel and basaltic melt. *Chemical Geology* **117,** 193–218.

Hunter, R. H. & Sparks, R. S. J. (1987). The differentiation of the Skaergaard intrusion. *Contributions to Mineralogy and Petrology* **95,** 451–461.

Jansen, B., Blok, A. & Scheelings, M. (1985). Geothermometry and geobarometry in Rogaland and preliminary results from the Bamble area, south Norway. In: Tobi, A. & Touret, J. L. R. (eds) *The Deep Proterozoic Crust in the North Atlantic Provinces. NATO Advanced Study Institute C158*. Dordrecht: D. Reidel, pp. 499–518.

Jensen, J., Nielsen, F., Duchesne, J., Demaiffe, D. & Wilson, J. (1993). Magma influx and mixing in the Bjerkreim–Sokndal layered intrusion, south Norway: evidence from the boundary between two macrocyclic units at Storeknuten. *Lithos* **29,** 311–325.

Johnson, K. T. M. & Kinzler, R. J. (1989). Partitioning of REE, Ti, Zr, Hf, and Nb between clinopyroxene and basaltic liquid: an ion microprobe study. *EOS Transactions, American Geophysical Union* **70,** 1388.

Kennedy, A. K., Lofgren, G. E. & Wasserburg, G. J. (1993). An experimental study of trace element partitioning between olivine, orthopyroxene and melt in chondrules: equilibrium values and kinetic effects. *Earth and Planetary Science Letters* **115,** 177–195.

Kolker, A. & Lindsley, D. H. (1989). Geochemical evolution of the Maloin Ranch pluton, Laramie Anorthosite Complex, Wyoming: petrology and mixing relations. *American Mineralogist* **74,** 307–324.

Kolker, A., Lindsley, D. H. & Hanson, G. N. (1990). Geochemical evolution of the Maloin Ranch pluton, Laramie Anorthosite Complex, Wyoming: trace elements and petrogenetic models. *American Mineralogist* **75,** 572–588.

Krause, H. & Pedall, G. (1980). Fe–Ti mineralizations in the Åna–Sira anorthosite, southern Norway. Metallogeny of the Baltic shield. In: Joako-Siivola (ed.) *Geological Survey of Finland Bulletin* **307,** 56–83.

Longhi, J. (1991). Comparative liquidus equilibria of hypersthene normative basalts at low pressure. *American Mineralogist* **76,** 785–800.

Longhi, J. & Vander Auwera, J. (1992). Polybaric fractionation and the connection between high-Al gabbro and monzonorite (abstract). *IGCP 290: Origin of Anorthosites and Related Rocks*, Liege: University of Liege.

McKay, G., Wagstaff, J. & Yang, S. R. (1986). Zirconium, Hafnium, and Rare Earth partition coefficients for ilmenite and other minerals in high-Ti lunar mare basalts: an experimental study. *Proceedings of the 16th Lunar and Planetary Science Conference. Journal of Geophysical Research* **91,** Supplement, D229–D237.

McKay, G. A. (1989). Partitioning of rare earth elements between major silicate minerals and basaltic melts. In: Lipin, B. R. & McKay, G. A. (eds) *Geochemistry and Mineralogy of Rare-earth Elements. Mineralogical Society of America, Reviews in Mineralogy* **21,** 45–78.

McLelland, J., Ashwal, L. & Moore, L. (1994). Composition and petrogenesis of oxide-, apatite-rich gabbronorites associated with Proterozoic anorthosite massifs: example from the Adirondack Mountains, New York. *Contributions to Mineralogy and Petrology* **116,** 225–238.

Michot, J. & Michot, P. (1969). The problem of anorthosites. In: Isachsen, Y. (ed.) *Origin of Anorthosites and Related Rocks. New York State Museum Science Service, Memoir* **18,** 399–410.

Michot, P. (1960). La géologie de la catazone: le problème des anorthosites, la palingenèse basique et la tectonique catazonale dans le Rogaland méridional (Norvège méridionale). *Norges Geologisk Undersøkelse* **212,** 1–54.

Mitchell, J. N., Scoates, J. S., Frost, C. D. & Kolker, A. (1996). The geochemical evolution of anorthosite residual magmas in the Laramie Anorthosite Complex, Wyoming. *Journal of Petrology* **37,** 637–660.

Morse, S. A. (1982). A partisan review of Proterozoic Anorthosites. *American Mineralogist* **65,** 1087–1100.

Nakamura, Y., Fujimaki, H., Nakamura, N., Tatsumoto, M., McKay, G. & Wagstaff, J. (1986). Hf, Zr, and REE partition coefficients between ilmenite and liquid: implications for lunar petrogenesis. *Proceedings of the 16th Lunar and Planetary Science Conference. Journal of Geophysical Research* **91,** Supplement D239–D250.

Nielsen, R. L. (1990). Simulation of igneous differentiation processes. In: Nicholls, J. & Russell, J. K. (eds) *Modern Methods of Igneous Petrology: Understanding Magmatic Processes. Mineralogical Society of America, Reviews in Mineralogy* **24,** 65–105.

Nielsen, R. L., Forsythe, L. M., Gallahan, W. E. & Fisk, M. R. (1994). Major- and trace-element magnetite–melt equilibria. *Chemical Geology* **117,** 167–191.

Owens, B. E. & Dymek, R. F. (1992). Fe–Ti–P-rich rocks and massif anorthosite: problems and interpretation illustrated from the Labrieville and St-Urbain pluton. *Canadian Mineralogist* **30,** 163–190.

Owens, B. E., Rockow, M. W. & Dymek, R. F. (1993). Jotunites from the Grenville Province, Quebec: petrological characteristics and implications for massif anorthosite petrogenesis. *Lithos* **30,** 57–80.

Philpotts, A. R. (1981). A model for the generation of massif-type anorthosites. *Canadian Mineralogist* **19,** 233–253.

Phinney, W. C. & Morrison, D. A. (1990). Partition coefficients for calcic plagioclase: implications for Archean anorthosites. *Geochimica et Cosmochimica Acta* **54,** 1639–1654.

Ray, G. L., Shimizu, N. & Hart, S. R. (1983). An ion microprobe study of the partitioning of trace elements between clinopyroxene and liquid in the system diopside–albite–anorthite. *Geochimica et Cosmochimica Acta* **47,** 2131–2140.

Roedder, E. (1979). Silicate liquid immiscibility in magmas. In: Yoder, H. S. (ed.) *The Evolution of the Igneous Rocks*. Princeton, NJ: Princeton University Press, pp. 15–57.

Schärer, U., Wilmart, E. & Duchesne, J. C. (1996). The short duration and anorogenic character of anorthosite magmatism: U–Pb dating of the Rogaland complex, Norway. *Earth and Planetary Science Letters* **139,** 335–350.

Steele, I. M. & Lindstrom, D. J. (1981). Ni partitioning between diopside and silicate melt: a redetermination by ion microprobe and recognition of an experimental complication. *Geochimica et Cosmochimica Acta* **45,** 2177–2183.

Sun, S. S. & McDonough, W. F. (1989). Chemical and isotopic systematics of oceanic basalts: implications for mantle composition and processes. In: Saunders, A. D. & Norry, M. J. (eds) *Magmatism*

in the Ocean Basins. *Geological Society, London, Special Publication* **42,** 313–345.

Thompson, R. N. (1982). British Tertiary volcanic province. *Scottish Journal of Geology* **18,** 49–107.

Toplis, M. J. & Carroll, M. R. (1996). Differentiation of ferro-basaltic magmas under conditions open and closed to oxygen: implications for the Skaergaard intrusion and other natural systems. *Journal of Petrology* **37,** 837–858.

Vander Auwera, J. & Longhi, J. (1994). Experimental study of a jotunite (hypersthene monzodiorite): constraints on the parent magma composition and crystallization conditions (P, T, fO_2) of the Bjerkreim–Sokndal layered intrusion (Norway). *Contributions to Mineralogy and Petrology* **118,** 60–78.

Vander Auwera, J., Longhi, J. & Duchesne, J. C. (1993). Jotunites from the Rogaland Province (Norway): constraints from experimental data and the partitioning of Sr (plag/melt) and Cr (opx/melt). *EOS Transactions, American Geophysical Union* **74,** 659.

Vander Auwera, J., Bologne, G., Roelandts, I. & Duchesne, J. C. (1998). Inductively coupled plasma-mass spectrometry (ICP-MS) analysis of silicate rocks and minerals. *Annales de la Société Géologique de Belgique* (in press).

Watson, E. B. (1976). Two-liquid partition coefficients: experimental data and geochemical implications. *Contributions to Mineralogy and Petrology* **56,** 119–134.

Watson, E. B. & Green, T. H. (1981). Apatite/liquid partition coefficients for REE and Sr. *Earth and Planetary Science Letters* **56,** 405–421.

Wiebe, R. A. (1979). Fractionation and liquid immiscibility in an anorthositic pluton of the Nain Complex, Labrador. *Journal of Petrology* **20,** 239–269.

Wiebe, R. A. (1990). Dioritic rocks in the Nain complex, Labrador. *Schweizerische Mineralogische und Petrographische Mitteilungen* **70,** 199–208.

Wilmart, E. (1988). Étude géochimique des charnockites du Rogaland (Norvège méridionale). *Mémoire en Sciences de la Terre, Université Pierre et Marie Curie, Paris* **88-20,** 341 pp.

Wilmart, E., Demaiffe, D. & Duchesne, J. C. (1989). Geochemical constraints on the genesis of the Tellnes ilmenite deposit, southwest Norway. *Economic Geology* **84,** 1047–1056.

Wilson, J. R., Robins, B., Nielsen, F. M., Duchesne, J. C. & Vander Auwera, J. (1996). The Bjerkreim–Sokndal layered intrusion, Southwest Norway. In: Cawthorn, R. G. (ed.) *Layered Intrusions*. Amsterdam: Elsevier, pp. 231–255.